molecules

MDPI

Review

A Review of Mn-Based Catalysts for Abating NO_x and CO in Low-Temperature Flue Gas: Performance and Mechanisms

Xiaodi Li [1], Shan Ren [1,*], Zhichao Chen [1], Mingming Wang [1], Lin Chen [1], Hongsheng Chen [1,*] and Xitao Yin [2]

[1] College of Materials Science and Engineering, Chongqing University, Chongqing 400044, China; lxd199611@126.com (X.L.); 20162749@cqu.edu.cn (Z.C.); 202009131184@cqu.edu.cn (M.W.); 13388961649@163.com (L.C.); yxtaj@163.com (X.Y.)

[2] School of Physics and Optoelectronic Engineering, Ludong University, Yantai 264000, China

* Correspondence: shan.ren@cqu.edu.cn (S.R.); chs@cqu.edu.cn (H.C.)

Abstract: Mn-based catalysts have attracted significant attention in the field of catalytic research, particularly in NO_x catalytic reductions and CO catalytic oxidation, owing to their good catalytic activity at low temperatures. In this review, we summarize the recent progress of Mn-based catalysts for the removal of NO_x and CO. The effects of crystallinity, valence states, morphology, and active component dispersion on the catalytic performance of Mn-based catalysts are thoroughly reviewed. This review delves into the reaction mechanisms of Mn-based catalysts for NO_x reduction, CO oxidation, and the simultaneous removal of NO_x and CO. Finally, according to the catalytic performance of Mn-based catalysts and the challenges faced, a possible perspective and direction for Mn-based catalysts for abating NO_x and CO is proposed. And we expect that this review can serve as a reference for the catalytic treatment of NO_x and CO in future studies and applications.

Keywords: Mn-based catalysts; NO_x catalytic reduction; CO catalytic oxidation; reaction mechanism

Citation: Li, X.; Ren, S.; Chen, Z.; Wang, M.; Chen, L.; Chen, H.; Yin, X. A Review of Mn-Based Catalysts for Abating NO_x and CO in Low-Temperature Flue Gas: Performance and Mechanisms. *Molecules* **2023**, *28*, 6885. https://doi.org/10.3390/molecules28196885

Academic Editors: Ioannis V. Yentekakis and Wai Lun Man

Received: 29 July 2023
Revised: 9 September 2023
Accepted: 26 September 2023
Published: 30 September 2023

1. Introduction

As the primary pollutants emitted from sintering, the coking and cement industries, etc., nitrogen oxides (NO_x) and carbon monoxide (CO) are harmful to both the environment and human health, often leading to acid rain, photochemical smog, ozone depletion, global warming, and so on [1,2]. Consequently, many scholars have focused their efforts on exploring effective strategies for removing these pollutants [3–6]. Among the available technologies, selective catalytic reduction (SCR) using NH_3 as the reducing agent was identified as an effective and reliable method for mitigating NO_x emissions [7]. Additionally, CO catalytic oxidation is also considered as a pivotal method for reducing hazardous exhaust emissions [8]. However, the lack of good-performance catalysts restricts the extensive utilizations of NH_3-SCR and CO catalytic oxidation technologies.

For the NH_3-SCR reaction, V_2O_5-$WO_3(MoO_3)/TiO_2$ catalysts have been commercially employed in power plants due to their excellent de-NO_x performance within the temperature range of 300–400 °C. Nevertheless, the narrow working temperature window and poor SCR activity at lower temperatures have constrained the application of this method in low-temperature flue gas denitrification. Additionally, Cu-CHA catalysts have been commercially used in vehicles due to their superior SCR activity and hydrothermal stability [9]. Nevertheless, Cu-CHA catalysts are sensitive to sulfur oxides, resulting in a significant decrease in SCR activity at lower temperatures [10,11]. As for CO catalytic oxidation, noble metal catalysts, including Au [12], Pt [13,14], Pd [15], etc., have been extensively employed to remove CO. Noble metal catalysts display a higher intrinsic activity for the conversion of CO and demonstrate good resistance to sulfur poisoning at lower temperatures [16]. However, noble metal catalysts also present some disadvantages. For instance, they are chemically sensitive and might degrade rapidly in the presence of

impurities [17]. Furthermore, they also show poor catalytic activity at lower temperatures [18]. Comparing transition metal and noble metal catalysts, it has been found that they could control CO almost equally, provided that the transition metal catalysts are used in larger volumes [19]. Therefore, transition metal catalysts have been considered as a promising alternative [20,21]. Among the transition metal oxide catalysts, Mn-based catalysts have attracted much attention due to their good low-temperature redox property [22]. However, Mn-based catalysts are easily poisoned by SO_2 and H_2O at lower temperatures and suffer from a low N_2 selectivity at higher temperatures in the NH_3-SCR reaction, as well as a narrow operating window [23]. Therefore, great efforts have been made to improve the catalytic performance and widen the temperature window [24,25]. Although some review articles have discussed the NH_3-SCR reaction over Mn-based catalysts, a systematic summary of Mn-based catalysts for NO_x catalytic reductions and CO catalytic oxidation is still missing. Hence, this review aimed to present a comprehensive review for the progress of Mn-based catalysts for both NH_3-SCR reactions and CO catalytic oxidation processes. In this review, the catalytic performance, reaction mechanisms, and interaction effects of the catalytic process for NO_x and CO are summarized. Furthermore, the crucial factors which influence the catalytic activity of Mn-based catalysts for NO reduction and CO oxidation are systematically identified. The structure diagram of this review is elucidated in Figure 1.

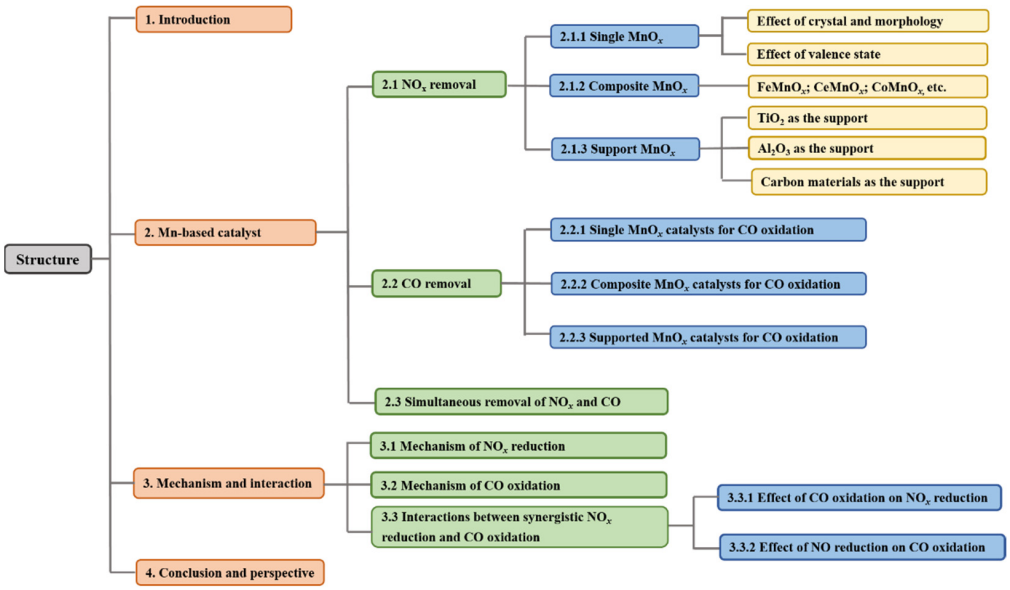

Figure 1. Structure diagram of this review.

2. Mn-Based Catalysts for Abating NO_x and CO

2.1. NO_x Removal

As low-temperature SCR catalysts, manganese oxide catalysts have exhibited great potential for NO_x reduction due to their diverse crystal structures and diverse metallization valences. However, pure MnO_x catalysts have the disadvantages of poor anti-SO_2 and H_2O catalytic activities and an inferior N_2 selectivity, which restrict their further applications. To address these shortcomings, some researchers have made efforts to enhance the SCR catalytic performance by forming other mixed oxides, such as transition or rare earth metal oxides, regulating the morphology and structure, and introducing suitable supports for the catalysts [26,27].

2.1.1. Single Mn Oxide Catalysts for NO_x Removal

(1) Effect of crystal phase and morphology

The SCR catalytic performance of manganese oxide catalysts is influenced by several key factors, including the oxidation state, crystallinity, specific surface area, and

morphology [28–31]. And these factors exert crucial influences on the catalysts' catalytic performance to varying degrees. Manganese oxides are composed of octahedral [MnO_6] units, which could form diverse arrays of tunnels and layered structures through the sharing of corners or edges [32,33]. These crystalline MnO_2 materials (α-, β-, δ-, γ-, λ-, and ε-MnO_2) can be categorized into three primary groups based on their structures: 1D, 2D, and 3D mesh structures, respectively. The 1D tunnel structures include α-, β-, and γ-MnO_2, each of which feature different tunnel arrangements: 1D (1 × 1) (2 × 2), (1 × 1), and (1 × 1) (1 × 2) tunnel, respectively. ε-MnO_2, which is similar to γ-MnO_2, exhibits a tunnel structure with highly disordered manganese lattice points and an irregular tunnel shape. δ-MnO_2 exhibits 2D-layered structures formed by the shared side of the [MnO_6] octahedron. On the other hand, λ-MnO_2 shows a typical spinel structure, characterized by a 3D (1 × 1) tunnel arrangement [34,35]. Figure 2 illustrates the schematics of different MnO_2 crystal structures, suggesting their unique arrangements and configurations [36].

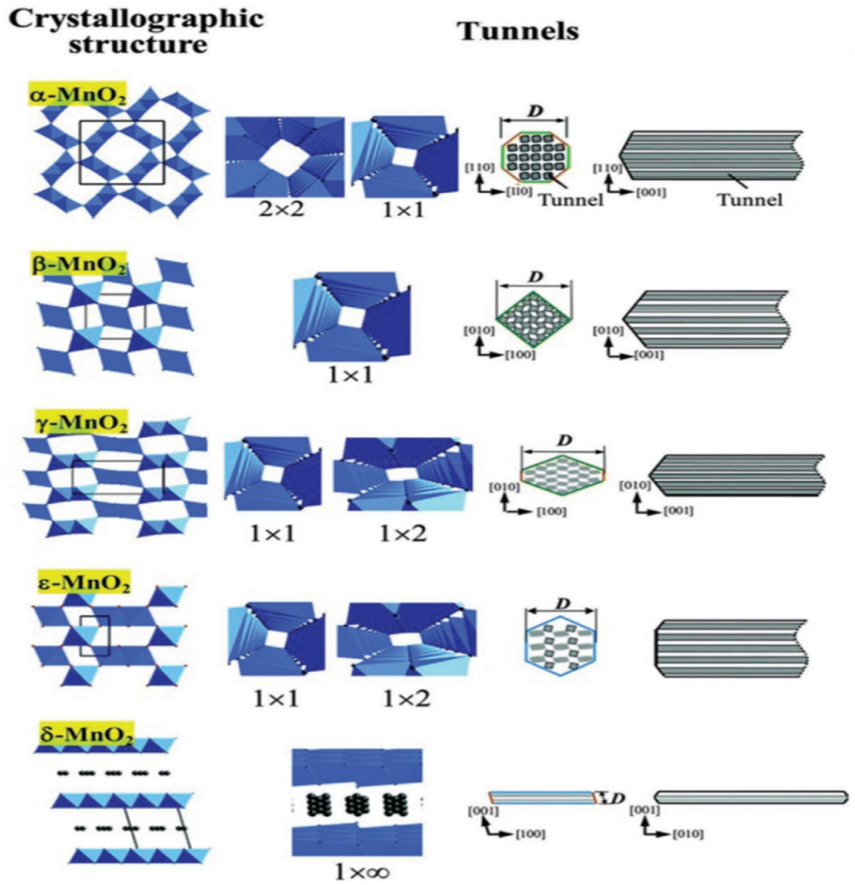

Figure 2. Structural models of various crystalline MnO_2 formations [36].

It has been reported that crystal structures could significantly influence the NO_x conversion efficiency of MnO_2 catalysts [37]. Dai et al. [38] suggested that α-MnO_2 catalysts display a higher de-NO_x activity compared to δ-MnO_2 catalysts, primarily due to them being assigned a higher abundance of surface chemisorbed oxygen species. Yang et al. [39] indicated that the NH_3 species adsorbed at Lewis sites on β-MnO_2 catalysts exhibited poor reactivity with O_2, resulting in less N_2O formation and a lower NO conversion. And the catalytic performance of γ-, α-, and δ-MnO_2 catalysts were also investigated (Figure 3). Furthermore, a range of MnO_2 catalysts with various morphologies, including MnO_2 nanorods, nanospheres, nanowire, nanotubes, nanoflower, mesoporous MnO_2 nanosheets, and 3D mesoporous MnO_2, were synthesized for removing NO_x [40–43]. Li et al. [44] synthesized MnO_2 nanomaterials with various morphologies via the hydrothermal method, as illustrated in Figure 4. The results indicated that the NO conversion efficiency decreased

in the following order: nanospheres > nanosheets > nanorods for MnO_2, and the removal efficiency of NO for the MnO_2 nanosphere catalyst could reach nearly 100% over the temperature range of 200 to 350 °C. Gao et al. [45] successfully synthesized mesoporous MnO_2 catalysts by employing KIT-6, SBA-15, and MCM-41 mesoporous silica as the templates. Among them, the mesoporous MnO_2-KIT-6 catalyst, characterized by 3D cubic channels, exhibited the highest NH_3-SCR activity and the widest temperature window.

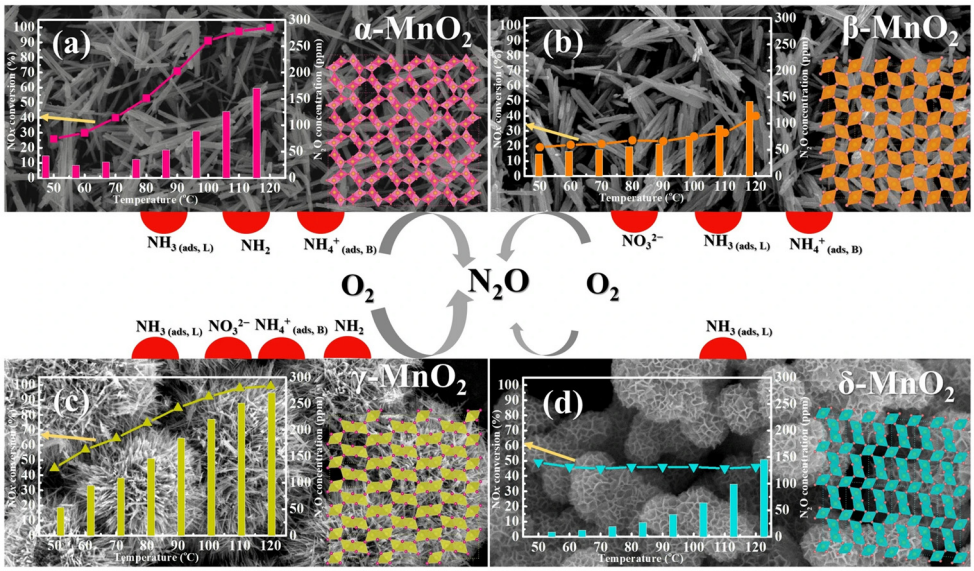

Figure 3. Catalytic activity and SEM diagrams of (**a**) α-MnO_2, (**b**) β-MnO_2, (**c**) γ-MnO_2, and (**d**) δ-MnO_2 catalysts [39].

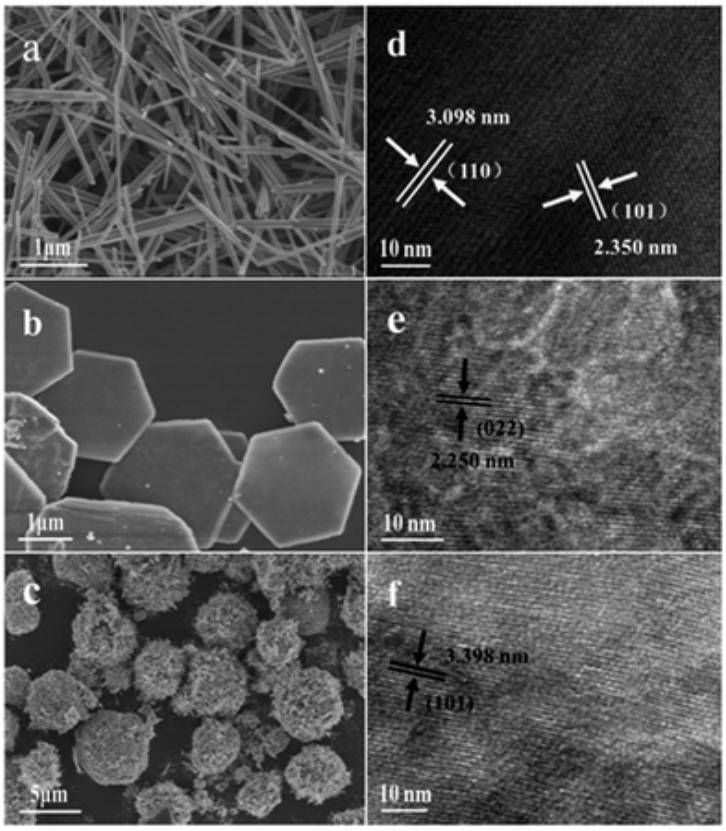

Figure 4. SEM and HRTEM images of (**a**,**d**) MnO_2 nanorods, (**b**,**e**) MnO_2 nanosheets, and (**c**,**f**) MnO_2 nanospheres [44].

(2) Effect of valence state

Each valence state of manganese is associated with a stable oxide, including MnO, Mn_2O_3, Mn_5O_8, Mn_4O_3, and MnO_2. The good de-NO_x activity of MnO_x catalysts at lower temperatures could be attributed to the presence of the multivalent oxidation state of manganese and high mobility of lattice oxygen [46–48]. Additionally, Yang et al. [48] conducted a study on the pathways of N_2O formation during an NH_3-SCR reaction over different valence states of manganese oxide catalysts, as depicted in Figure 5. It could be observed that the MnO_2 catalysts yielded more N_2O at lower temperatures. In situ DRIFTS results indicated that the most of the N_2O was generated from the SCR reaction on the MnO_2 catalysts at lower temperatures, and the N_2O amounts produced via the NH_3 oxidation of the catalyst increased with the rising temperature. Wan et al. [49] emphasized the significance of Mn^{4+} species as the primary active species in the NH_3-SCR reaction. These findings were also confirmed by the studies of Zhang et al. [50] and Pappas et al. [51].

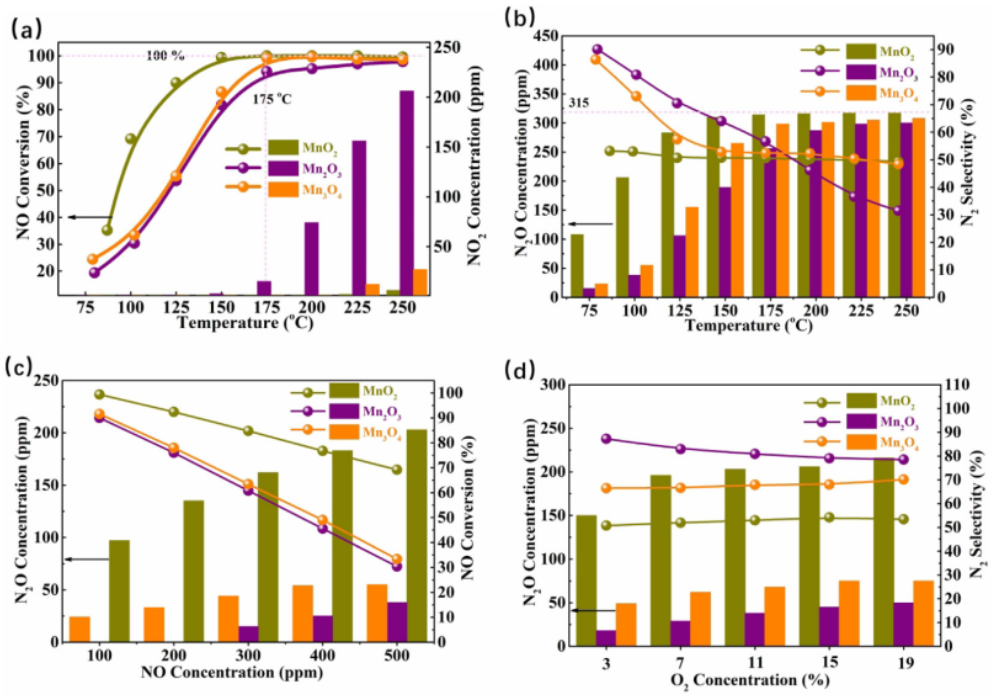

Figure 5. (**a**) SCR activity, (**b**) N_2O concentration and N_2 selectivity of catalysts at different temperature, (**c**) N_2O concentration and NO conversion, and (**d**) N_2O concentrations and N_2 selectivity of catalysts at different NO and O_2 concentrations [48].

2.1.2. Composite MnO_x Catalysts for NO_x Removal

As for the stringent emission standards for NO_x, relying solely on a single MnO_x catalyst in the NH_3-SCR system is not sufficient to meet the discharge requirements. Mixing or doping MnO_x with other metal oxides can enhance the catalytic activity of MnO_x catalysts, owing to the synergistic effects achieved by combining Mn and other metal elements. Transition metal oxides, such as Fe_2O_3, CeO_2, Co_3O_4, CuO, etc., have been widely employed for the modification of MnO_x catalysts [52–54]. The incorporation of other metal oxides usually generates abundant active sites, rich oxygen vacancies, and an excellent redox capacity, all of which contribute to the enhancement of the catalytic performance [55–57]. For instance, Shi et al. [58] synthesized Mn-based bimetallic transition oxide catalysts and investigated the impact of various transition metals on the catalytic activity of pure MnO_x catalysts. As illustrated in Figure 6, the Co-MnO_x catalyst achieved about a 95% NO conversion efficiency at 100 °C. This superior catalytic activity of the Co-MnO_x catalyst was likely attributed to the unique manganese-rich surface activity. Kang et al. [59] synthesized a Ni-doped MnO_x catalyst using the solvent-free doping

method and evaluated its SCR performance. The result suggested that Ni doping could enhance the medium-temperature activity, obtaining a remarkable 100% NO conversion rate at 100–200 °C. Jiang et al. [60] suggested that the incorporation of Zr could improve the catalytic activity and SO_2 tolerance of Mn-based catalysts. The characterization results revealed that the introduction of Zr strengthened the interaction between Zr and the active sites, resulting in the amorphous structure of the catalysts. Moreover, in situ DRIFTS studies displayed that the addition of Zr promoted the L-H reaction pathways at lower temperatures. Long et al. [61] indicated that the co-doping of Nb and Fe optimized the low-temperature SCR activity and N_2 selectivity of $MnCeO_x$ catalysts, as depicted in Figure 7.

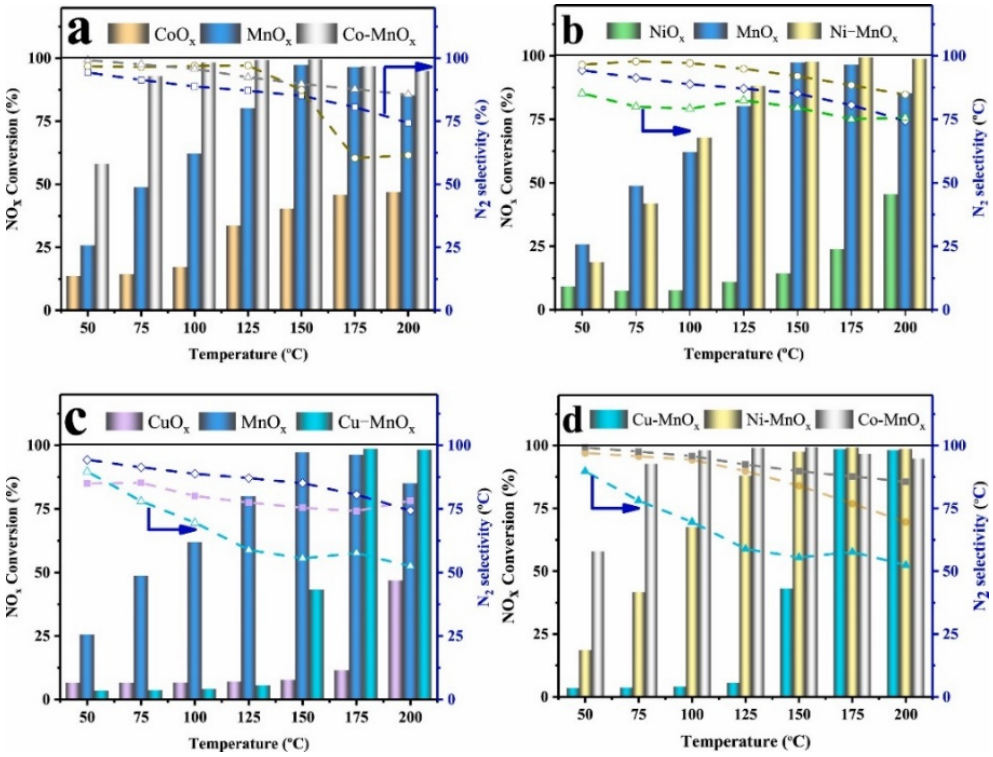

Figure 6. Influence of different metal oxides as additives on the catalytic activity of a MnO_x catalyst: (**a**) CoO_x, MnO_x, and Co-MnO_x; (**b**) NiO_x, MnO_x, and Ni-MnO_x; (**c**) CuO_x, MnO_x, and Cu-MnO_x; (**d**) Cu-MnO_x, Ni-MnO_x, and Co-MnO_x [58].

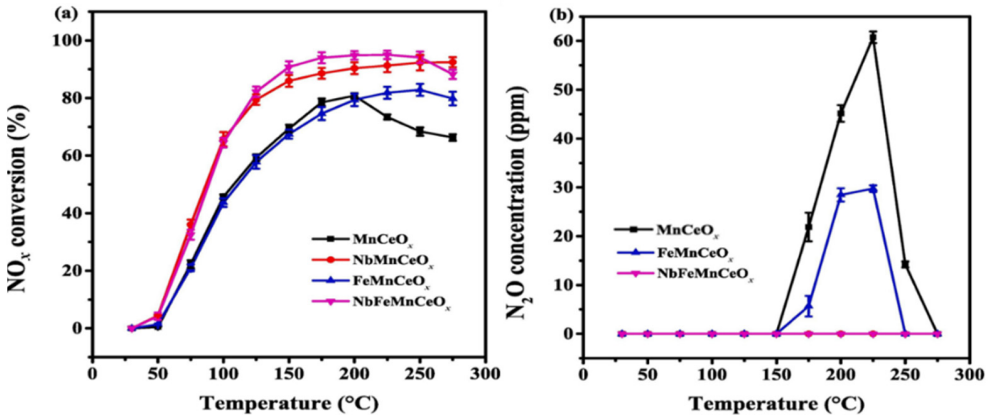

Figure 7. (**a**) NO_x conversion and (**b**) N_2O concentration over Mn-based oxide catalysts [61].

2.1.3. Supported MnO_x Catalysts for NO_x Removal

The choice of suitable supports has a profound impact on shaping the crystalline and catalytic performance of NH_3-SCR catalysts. An ideal support not only provides a large specific surface area for the efficient dispersion of the active components, but also creates a favorable environment for catalytic reactions to occur. To date, extensive efforts have been dedicated to exploring various support materials, including TiO_2 [62,63], Al_2O_3 [64–66], CeO_2 [67–69], SiO_2 [70], ZrO_2 [71,72], and active carbon (AC) [21,73], as potential supports for the immobilization of MnO_x catalysts.

(1) TiO_2 as support

TiO_2 as a support has demonstrated an excellent resistance to SO_2 [74]. Moreover, it can interact with MnO_x catalysts to enhance the dispersion of Mn species [75,76]. Smirniotis et al. [77] investigated the impact of different TiO_2 phases on the SCR catalytic activity of MnO_2/TiO_2 catalysts. The result indicated that MnO_x/TiO_2 (hombikat, anatase) displayed the highest SCR activity, attributed to the larger specific surface area and abundant acid sites of TiO_2 (hombikat, anatase). Li et al. [74] prepared Mn-Ce/TiO_2-NS and Mn-Ce/TiO_2-NP catalysts, utilizing anatase TiO_2 with exposed {001} crystal faces (TiO_2-Ns) and anatase TiO_2 with exposed {101} crystal faces (TiO_2-NP) as supports, respectively. The Mn-Ce/TiO_2-NS catalyst exhibited higher SCR activity than that of the Mn-Ce/TiO_2-NP catalyst, even in the presence of SO_2, as illustrated in Figure 8. This was due to the anatase TiO_2 {001} facets potentially preferentially reacting with SO_2, thus avoiding the inactivation of the active sites.

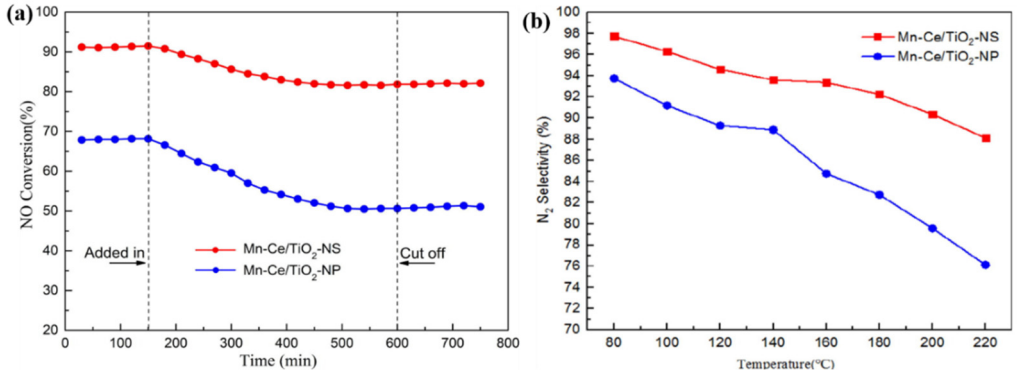

Figure 8. (**a**) SCR performance in the presence of SO_2 and (**b**) N_2 selectivity for two kinds of Mn-Ce/TiO_2 catalysts [74].

(2) Al_2O_3 as support

A large surface area, abundant acid sites, and a superior mechanical property makes Al_2O_3 an outstanding support for SCR catalysts. Yao et al. [78] synthesized MnO_x catalysts with different supports, and the influence of these supports on the physicochemical properties and denitration performance of the catalysts was evaluated. The results indicated that the MnO_x/γ-Al_2O_3 catalyst exhibited a strong NO_x adsorption capacity and had abundant Mn^{4+} species, resulting in a higher SCR activity in the entire reaction temperature (Figure 9). Furthermore, comparative studies on Mn-Ce oxides supported on TiO_2 and Al_2O_3 for NH_3-SCR at low temperatures were conducted by Jin et al. [79]. The results demonstrated that the Mn-Ce/Al_2O_3 catalyst showed a relatively higher SCR activity than the Mn-Ce/TiO_2 catalyst at the temperature range of 80–150 °C, primarily due to the Mn-Ce/Al_2O_3 catalyst having more acid sites. Li et al. [80] synthesized supported catalysts of FeO_x and MnO_x that were co-supported on aluminum-modified CeO_2 for a low-temperature NH_3-SCR reduction of NO_x. It was observed that the Fe-Mn/Ce_1Al_2 catalyst achieved over a 90% NO conversion at 75–250 °C and displayed superior SO_2 resistance compared to the Fe-Mn/CeO_2 catalyst. The improved catalytic performance

could be ascribed to the larger surface area, and the enhanced reducibility was due to the introduction of Al_2O_3.

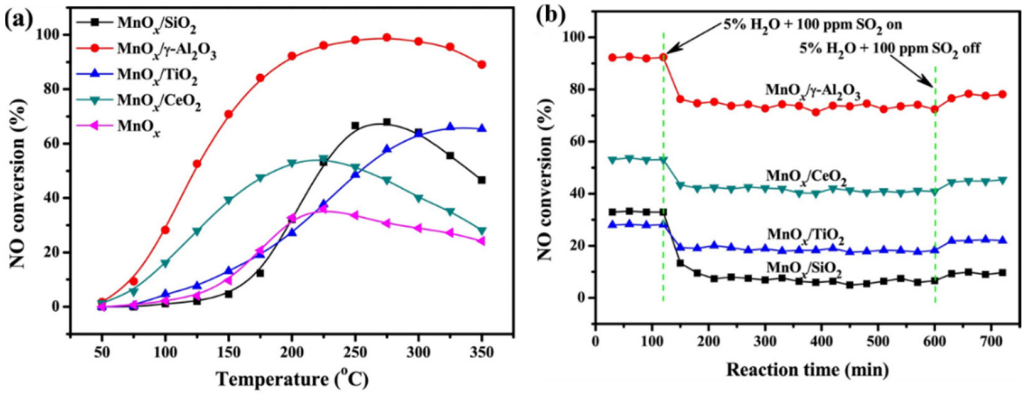

Figure 9. (**a**) NO conversion and (**b**) H_2O + SO_2 resistance at 200 °C for Mn-based catalysts with different supports [78].

(3) Carbon materials as support

Carbon materials, including carbon nanotubes (CNTs), activated carbon (AC), activated carbon fiber (ACF), and graphene (GR), have been identified as attractive supports for SCR catalysts [81,82]. Su et al. [83] synthesized a range of MnO_x catalysts supported by CNTs and assessed their SCR catalytic performance. The results showed that the catalyst with MnO_x introduced into the CNT channels demonstrated superior SCR activity compared to the MnO_x on the outside surface of the CNTs. Xiao et al. [84] reported that the denitration performance of a MnO_x-CeO_2/GR catalyst was better than that of a MnO_x-CeO_2 catalyst even in the presence of SO_2 and H_2O, as displayed in Figure 10. The result suggested that the introduction of GR altered the composition of the Mn species, thereby exerting a notable influence on the electron mobility. Jiang et al. [85] revealed that the introduction of AC into the catalyst resulted in an enhancement in the NO conversion efficiency. Table 1 summarizes the research results of Mn-based catalysts for NO catalytic reduction in recent years.

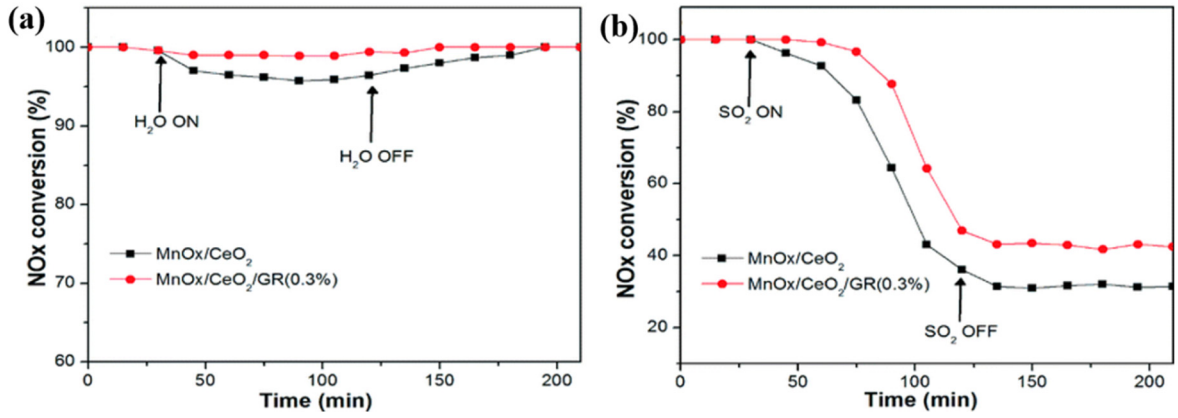

Figure 10. (**a**) H_2O and (**b**) SO_2 tolerance of MnO_x-CeO_2 and MnO_x-CeO_2/GR catalysts at 180 °C [84].

2.2. CO Removal

2.2.1. Single MnO_x Catalysts for CO Oxidation

Manganese oxide catalysts with different crystal structures and morphologies have exhibited significant differences in their catalytic performance for CO catalytic oxidation [86]. Xu et al. [87] reported that an α-MnO_2 nanowire catalyst exhibited higher catalytic activity than a β-MnO_2 catalyst, which was attributed to the α-MnO_2 catalyst possessing

a remarkable oxidation ability. Frey et al. [88] prepared non-stoichiometric MnO_x catalysts and studied the relationship between their micro-structural correlation and catalytic activity for CO oxidation. The results revealed that the excellent catalytic activity of the non-stoichiometric MnO_x catalyst could be attributed to the presence of nanocrystals at the ending of the nanorods. Additionally, earlier studies have indicated that the catalyst's reactivity is linked to the ability of Mn to form different oxidation states, such as the redox of Mn^{2+}/Mn^{3+} or Mn^{3+}/Mn^{4+}, as well as the mobility of lattice oxide species [89,90].

Table 1. Details of catalytic performance, preparation methods, and reaction conditions for Mn-based catalysts removing NO_x.

Catalysts	Preparation Method	Reaction Conditions	NO_x/NO Conversion (%)	T (°C)	References
α-MnO_2	Hydrothermal	0.1% NO, 0.1% NH_3, 2% O_2, N_2 as balance, 38,000 h^{-1}	90%	125 °C	[38]
γ-MnO_2	Hydrothermal	500 ppm NO, 500 ppm NH_3, 19% O_2, N_2 as balance, 36,000 h^{-1}	90%	100 °C	[39]
MnO_2 nanosphere	Hydrothermal	500 ppm NO, 500 ppm NH_3, 3% O_2, N_2 as balance, 28,000 h^{-1}	95%	150 °C	[44]
MnO_2-KIT-6	Impregnation	1000 ppm NO, 1000 ppm NH_3, 5% O_2, Ar as balance, 30,000 h^{-1}	98%	100 °C	[45]
MnO_2	Hydrothermal	500 ppm NO, 500 ppm NH_3, 19% O_2, N_2 as balance, 36,000 h^{-1}	100%	150 °C	[48]
Mn_3O_4	Hydrothermal	500 ppm NO, 500 ppm NH_3, 19% O_2, N_2 as balance, 36,000 h^{-1}	100%	175 °C	[48]
$Mn_{0.25}$/TNT-H	Hydrothermal	900 ppm NO, 100 ppm NO_2, 1000 ppm NH_3, 10% O_2, He as balance, 50,000 h^{-1}	100%	100 °C	[51]
$MnFeO_x$	Co-precipitation	500 ppm NO, 500 ppm NH_3, 5% O_2, N_2 as balance, 75,000 h^{-1}	100%	100 °C	[52]
MnCe nanowire	Hydrothermal+ co-precipitation	500 ppm NO, 500 ppm NH_3, 5% O_2, N_2 as balance, 32,000 h^{-1}	100%	150 °C	[44]
Co-MnO_x	Solvothermal	2000 ppm NO, 2000 ppm NH_3, 8% O_2, N_2 as balance, 128,000 h^{-1}	100%	100 °C	[58]
$NbFeMnCeO_x$	Co-precipitation	500 ppm NO, 500 ppm NH_3, 11% O_2, N_2 as balance, 60,000 h^{-1}	95%	175 °C	[61]
Mn/γ-Al_2O_3	Sol-gel	500 ppm NO, 500 ppm NH_3, 5% O_2, N_2 as balance, 60,000 h^{-1}	95%	200 °C	[78]
Mn-Ce/Al_2O_3	Impregnation	800 ppm NO, 800 ppm NH_3, 3% O_2, N_2 as balance, 120,000 h^{-1}	90%	180 °C	[79]
FeMn/CeAl	Impregnation	500 ppm NO, 500 ppm NH_3, 5% O_2, N_2 as balance, 30,000 h^{-1}	100%	100 °C	[80]
Ce-Mn/AC	Impregnation	500 ppm NO, 500 ppm NH_3, 5% O_2, N_2 as balance, 30,000 h^{-1}	95%	175 °C	[81]
Mn/CNT	Impregnation	0.08% NO, 0.08% ppm NH_3, 5% O_2, A_2 as balance, 35,000 h^{-1}	95%	200 °C	[83]
MnO_x-CeO_2/GR	Hydrothermal	500 ppm NO, 500 ppm NH_3, 5% O_2, N_2 as balance, 24,000 h^{-1}	100%	200 °C	[84]
Mn-Fe/Z-AC	Hydrothermal	450 ppm NO, 450 ppm NH_3, 5% O_2, N_2 as balance, 2,000 h^{-1}	98%	125 °C	[85]

2.2.2. Composite MnO_x Catalysts for CO Oxidation

Composite oxides consist of two or more active components, and the interaction between different active species can modify their dispersion state, ultimately leading to an enhanced catalytic activity and the stability of the catalysts. In comparison to a pure MnO_x catalyst, composite MnO_x catalysts have preferable crystal structures and redox properties, which exhibit higher catalytic activity in CO catalytic oxidation [91]. Pan et al. [92] found that CO conversion efficiency on MnO_x catalysts was significantly enhanced after introducing copper oxides. And the improved CO catalytic activity of

$CuMnO_x$ catalysts was related to the resonance system of $Cu^{2+}+Mn^{3+} \leftrightarrows Cu^{+}+Mn^{4+}$ and the efficient oxidation of CO onto Cu^{2+} and Mn^{4+} species. Zhang et al. [93] prepared a range of MnO_x-CeO_2 catalysts with varying Mn/Ce molar ratios and studied the catalytic activity for CO catalytic oxidation. It could be observed that a Mn_1Ce_1 catalyst showed a better catalytic performance and wider operating temperature window than pure MnO_x and CeO_2 catalysts.

2.2.3. Supported MnO_x Catalysts for CO Oxidation

Loading MnO_x on the support materials, such as TiO_2 [94,95], Al_2O_3 [96], and CeO_2 [68], provided a prospective practical application of Mn-based catalysts in CO catalytic oxidation. Dong et al. [94] designed a Mn_3O_4/TiO_2 catalyst grown in situ on a titanium mesh substrate for CO catalytic oxidation. As shown in Figure 11, the Mn_3O_4/TiO_2 catalyst achieved nearly complete CO conversion (100%) at a relatively low temperature of 160 °C, surpassing the performance of some noble metal catalysts. Li et al. [97] prepared $CuMn/Al_2O_3$ catalysts employing ordered mesoporous Al_2O_3 as a support. The result suggested that the ordered mesoporous Al_2O_3 led to catalysts with higher specific surface areas and large pore volumes, as well as more surface activity species, thereby enhancing the CO catalytic oxidation activity of the catalyst. A comprehensive summary of the research results of Mn-based catalysts for CO catalytic oxidation are presented in Table 2.

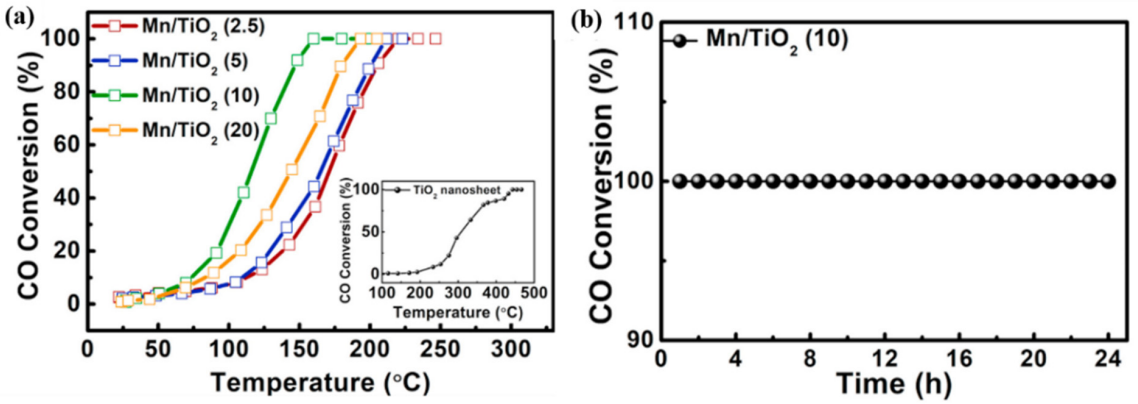

Figure 11. (**a**) CO conversion with temperature and (**b**) the CO oxidation stability of the Mn/TiO_2 catalyst [95].

Table 2. Details of catalytic performance, preparation methods, and reaction conditions for Mn-based catalysts removing CO.

Catalysts	Preparation Method	Reaction Condition	Best CO Conversion (%)	T (°C)	Reference
MnO_x-CeO_2	Co-precipitation	1% CO, 20% O_2, Ar as balance, 75,000 h^{-1}	100%	175 °C	[68]
α-MnO_2	Hydrothermal	2% CO, 98% air, 12,000 h^{-1}	100%	120 °C	[86]
β-MnO_2	Hydrothermal	1% CO, 16% O_2, N_2 as balance, 60,000 h^{-1}	90%	169 °C	[87]
Ce-MnO_2	Hydrothermal	1% CO, 10% O_2, N_2 as balance, 30,000 h^{-1}	100%	175 °C	[89]
Cu-MnO_x	Hydrothermal	1% CO, 0.6% O_2, He as balance, 150,000 h^{-1}	100%	150 °C	[92]
Mn_3O_4/TiO_2	Urea-assisted deposition	1% CO, 20% O_2, He as balance, 7200 h^{-1}	100%	150 °C	[94]
$CuMnO_x/\gamma$-Al_2O_3	Sol-gel + co-precipitation	2.5% CO, air as balance, 30,000 h^{-1}	100%	120 °C	[96]
CuMn-Al_2O_3	Co-precipitation	1% CO, air as balance, 10,000 h^{-1}	100%	120 °C	[97]

2.3. Simultaneous Removal of NO_x and CO

Nitrogen oxides and carbon monoxide coexist in the emissions of some plants, including coal-fired power plants, the steel industry, coking plants, and the cement industry. The development of bifunctional catalysts was of great importance for effectively removing both NO_x and CO simultaneously. Manganese-based catalysts exhibit a range of oxidation states and unstable oxygen species, which play a crucial role in enhancing the adsorption and activation of NO_x and CO on the catalyst surface [98,99]. In our earlier study [100], we found that γ-MnO_2 catalysts exhibit higher catalytic activity for both NO reduction and CO oxidation compared to α-, β-, and δ-MnO_2 catalysts (see Figure 12). And the outstanding catalytic performance of the γ-MnO_2 catalyst could be assigned to its remarkable redox property and abundant active sites, which promote the adsorption and activation of NO and CO molecules. Zheng et al. [101] prepared $CuMnO_x$ bifunctional catalysts and evaluated their catalytic performance for NO reduction and CO oxidation. As shown in Figure 13, a Cu_1Mn_1 catalyst exhibited excellent activity for removing NO and CO simultaneously, achieving nearly 100% NO conversion and 96% CO conversion at 125 °C, respectively. Gui et al. [102] reported a bifunctional catalyst of $Mn_2Cu_2Al_1O_x$ which possessed dual active sties and was highly active for both NH_3-SCR and CO oxidation reactions. The results indicated that CO was more easily adsorbed on the Cu active sites, while NH_3 was more inclined to absorb on the Mn active sites, which enabled the simultaneous occurrence of NO catalytic reduction and CO oxidation on the catalyst surface. Guo et al. [53] synthesized a CuMn-HZSM-5 catalyst via the impregnation method. The optimized catalyst achieved a 90% NO removal efficiency and nearly a 100% CO conversion rate at 200 °C. The results of the bifunctional catalysts for removing both NO_x and CO simultaneously are concluded in Table 3.

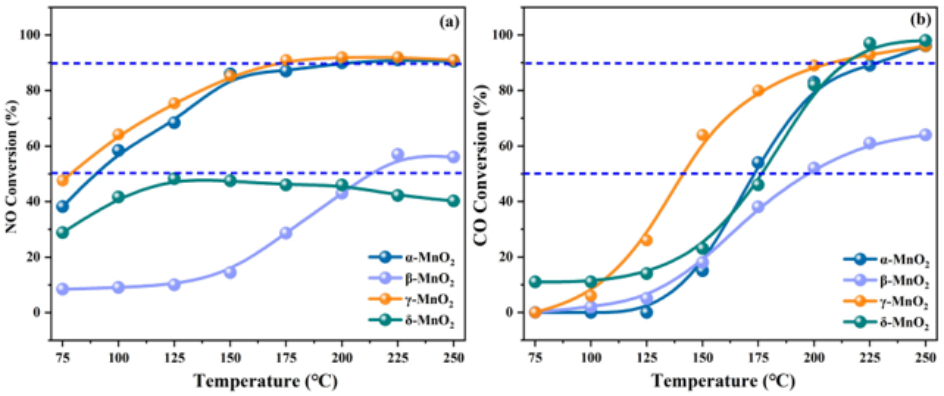

Figure 12. (**a**) NO conversion and (**b**) CO conversion over MnO_2 catalysts with different crystalline phases [100].

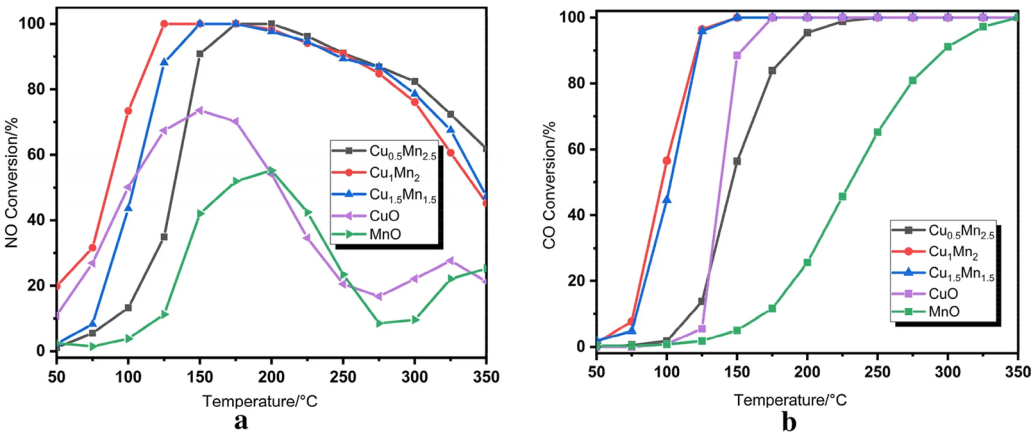

Figure 13. (**a**) NO conversion and (**b**) CO conversion of $CuMnO_x$ catalysts [101].

Table 3. Details of catalytic performance, preparation methods, and reaction conditions for Mn-based catalysts removing NO_x and CO.

Catalysts	Preparation Method	Reaction Conditions	NO_x Conversion (%)	CO Conversion (%)	T (°C)	Reference
CuMn-HZSM-5	Impregnation	500 ppm NO, 500 ppm NH_3, 5000 ppm CO, 5% O_2, N_2 as balance, 120,000 h^{-1}	90%	100%	200 °C	[53]
γ-MnO_2	Hydrothermal	500 ppm NO, 500 ppm NH_3, 1000 ppm CO, 11% O_2, N_2 as balance, 90,000 h^{-1}	91%	80%	175 °C	[100]
Cu_1Mn_2	Co-precipitation	500 ppm NO, 500 ppm NH_3, 2000 ppm CO, 5% O_2, N_2 as balance, 100,000 h^{-1}	96%	100%	125 °C	[101]
$Mn_2Cu_2Al_1O_x$	Aqueous miscible organic solvent treatment	500 ppm NO, 500 ppm NH_3, 5000 ppm CO, 5% O_2, Ar as balance, 80,000 h^{-1}	97%	100%	200 °C	[102]
$MnCuCeO_x$/γ-Al_2O_3	Impregnation	300 ppm NO, 300 ppm NH_3, 3000 ppm CO, 16% O_2, N_2 as balance, 25,000 h^{-1}	100%	100%	200 °C	[103]
$Mn_2Co_1O_x$/IM	Hydrothermal	500 ppm NO, 500 ppm NH_3, 5% O_2, 5000 ppm CO, A_2 as balance,	98%	100%	200 °C	[104]

3. Mechanisms and Interactions of NO_x Catalytic Reduction and CO Catalytic Oxidation

3.1. Pathways and Mechanisms of NO_x Catalytic Reduction on Mn-Based Catalysts

Understanding the pathways and mechanisms of NO_x catalytic reductions over the catalysts was of significance in attaining efficient denitrification. In the NH_3-SCR reaction, the primary pathways of NO_x reduction could be outlined using Equations (1)–(5):

$$4NO + 4NH_3 + O_2 \rightarrow 4N_2 + 6H_2O \quad (1)$$

$$4NH_3 + 2NO + 2NO_2 \rightarrow 4N_2 + 6H_2O \quad (2)$$

$$2NO_2 + 4NH_3 + O_2 \rightarrow 3N_2 + 6H_2O \quad (3)$$

$$6NO_2 + 4NH_3 \rightarrow 7N_2 + 12H_2O \quad (4)$$

$$6NO + 4NH_3 \rightarrow 5N_2 + 6H_2O \quad (5)$$

Among them, Reaction (1) was referred to as the "standard SCR" reaction, containing a stoichiometry with identical amounts of NO and NH_3. In the presence of NO_2, Reaction (2) proceeded at a higher rate compared to the "standard SCR", so it was defined as "fast SCR". When an excess of NO_2 ($NO_2/NO > 1$) was present in the flue gas, Reactions (3) and (4) happened. Reaction (5), between NH_3 and NO, proceeded in an oxygen-free or low-oxygen atmosphere.

The Eley–Rideal (E-R) and Langmuir–Hinshelwood (L-H) mechanisms are commonly accepted pathways in the NH_3-SCR reaction [105], as illustrated in Figure 14. As for the E-R mechanism, ammonia molecules are initially adsorbed at the acid sites on the catalyst

surface, leading to the formation of intermediates, such as -NH_2 species and adsorbed NH_3 species. Subsequently, these intermediates react with gaseous NO and NO_2, ultimately resulting in the generation of N_2 and H_2O. The reaction process can be described using Equations (6)–(10):

$$NH_{3(gas)} \rightarrow NH_{3(ads)} \quad (6)$$

$$NH_{3(ads)} + M^{n+} = O \rightarrow NH_{2(ads)} + M^{(n-1)+} - O - H \quad (7)$$

$$NH_{2(ads)} + M^{n+} = O \rightarrow NH_{(ads)} + M^{(n-1)+} - O - H \quad (8)$$

$$NH_{2(ads)} + NO_{(gas)} \rightarrow N_2 + H_2O \quad (9)$$

$$NH_{(ads)} + NO_{(gas)} \rightarrow N_2O + H^+ \quad (10)$$

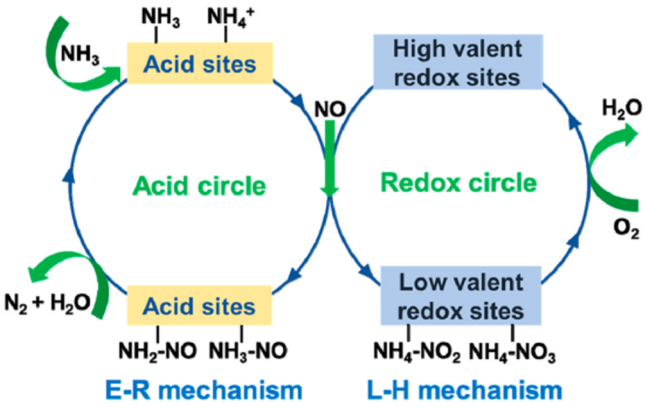

Figure 14. Schematic diagram of NH_3-SCR reaction pathways over the transition metal oxide catalysts [105].

Marbán et al. [106] found that Mn_3O_4/AC catalysts primarily follow the E-R mechanism in the NH_3-SCR reaction, in which NO_2 and, to a lesser extent, NO react with surface-active NH_3 species. Xu et al. [107] also proposed that the SCR reaction over a MnO_x catalyst proceeds via the E-R mechanism, in which the adsorbed NH_3 species could react with the gaseous NO. Chen et al. [52] confirmed that the E-R mechanism plays a more significant role in the SCR reaction over $MnFeO_x$ catalysts by employing the transient reaction experiments.

For the L-H mechanism, NO was adsorbed on the active sites of the catalyst to form NO_x adsorbed species. Then, the adsorbed NH_3 reacted with the adsorbed NO_x species to produce N_2 and H_2O. The specific processes are shown in Figure 15. In general, the L-H mechanism is easier to proceed with than the E-R mechanism owing to its low activation energy [108]. Kijlstra et al. [66] proposed that the Mn^{3+} site over the MnO_x/Al_2O_3 catalyst was the center of Lewis acid sites, and -NH_2 species were generated via the deamination of adsorbed NH_3 reacting with gaseous NO and adsorbed NO at the same time. That is, both the L-H and E-R mechanisms occurred. Wei et al. [109] explored the mechanism of a Mn/TiO_2 catalyst in the NH_3-SCR reaction via a series of experiments and DFT calculations. The result showed that the catalytic reaction pathway on the catalysts consisted of two fundamental steps, as illustrated in Figure 16.

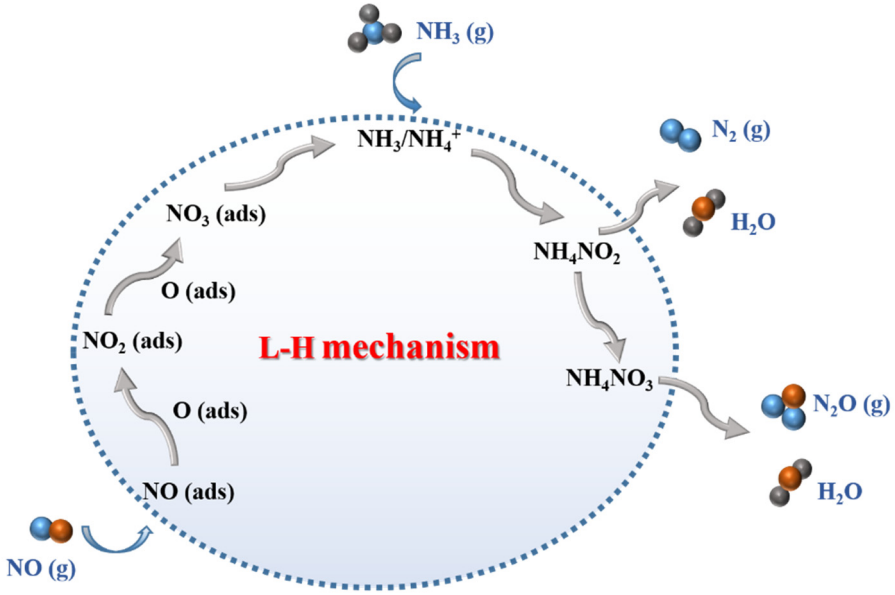

Figure 15. Schematic diagram of the L-H mechanism in the NH_3-SCR reaction over the catalysts.

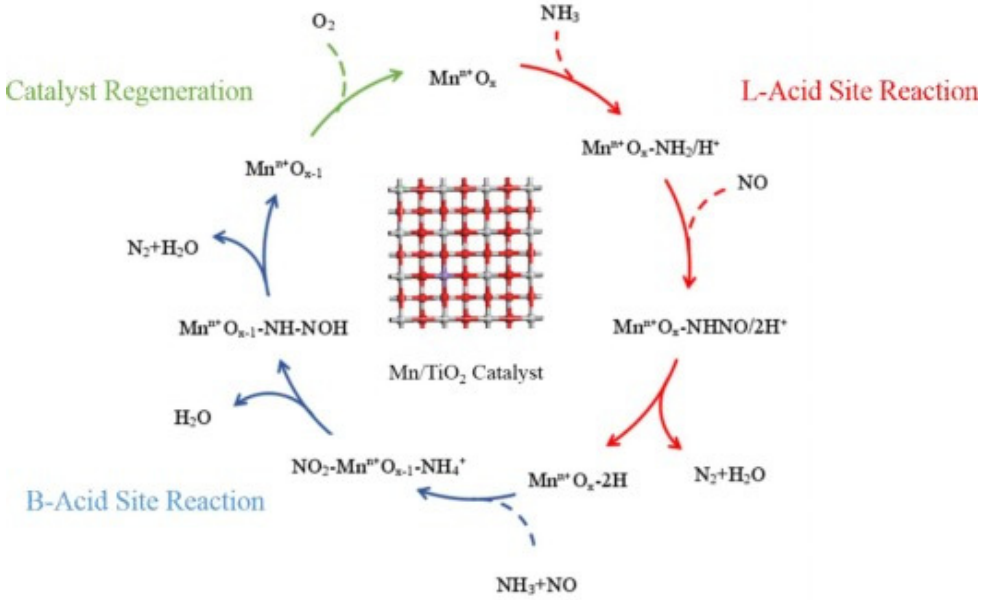

Figure 16. NH_3-SCR reaction mechanism over MnO_x/TiO_x catalysts [109].

3.2. Mechanisms of CO Oxidation on Mn-Based Catalysts

The catalytic oxidation of CO is one of the most representative prototype reactions in heterogeneous catalysis, and attracts significant interest due to its extensive applications in the environmental and energy fields. At present, the proposed mechanisms for CO catalytic oxidation mainly encompass the L-H, E-R, and Mars–van Krevelen (MvK) mechanisms [110–112], as depicted in Figure 17.

The L-H mechanism, as presented in Figure 17a, involves the following key steps: CO reacts with OH- on the catalyst surface, leading to the formation of formate or carbonate species. Subsequently, the adsorbed formate or carbonate species decompose to produce CO_2 and H_2. Then, the presence of metal catalysts facilitates the preferential adsorption of CO and promotes the easier breaking of C-H bonds in formate species. During this reaction process, the lattice oxygen does not participate in the catalytic oxidation, and the reaction occurs through the adsorption and reaction of CO and O_2 on the catalyst surface [111,113]. Dey et al. [114] proposed that $CuMnO_x$ catalysts predominantly follow the L-H mechanism

in the CO catalytic oxidation process, primarily involving the reaction of surface-activated oxygen species with adsorbed CO species to produce CO_2.

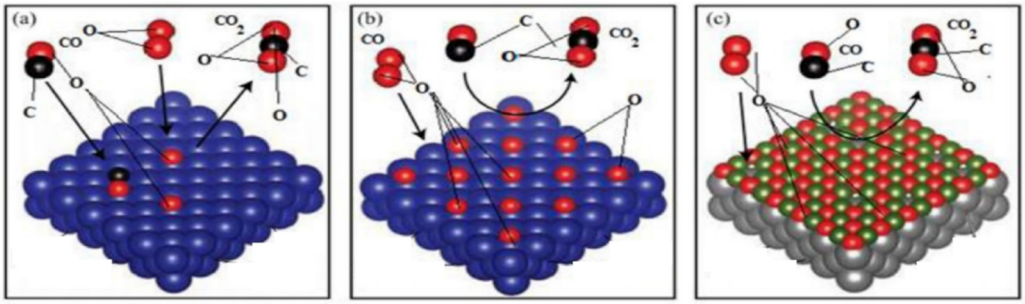

Figure 17. (**a**) L-H mechanism, (**b**) E-R mechanism, and (**c**) MvK mechanism diagrams for CO oxidation [115].

The E-R mechanism is displayed in Figure 17b. The mechanism involves the reaction that occurs between gaseous CO molecules and chemisorbed oxygen species (atomic oxygen and molecular oxygen). The MvK mechanism is also known as the redox mechanism, as illustrated in Figure 17c. In this mechanism, the catalyst surface exhibits a preference for the adsorption of activated CO molecules, which then react with lattice oxygen, resulting in the formation of CO_2 and the creation of oxygen vacancies on the catalyst surface [115]. Subsequently, gaseous oxygen enters the oxygen vacancies and reacts with the partially reduced catalyst, replenishing its oxidation capacity [116]. The redox reaction mechanism involves two types of active sites: (1) active metal cation sites, which are responsible for oxidizing the reactants, and (2) active sites for the reduction of molecular oxygen. Typically, transition metal ions exhibit excellent electron conductivity, which facilitates efficient electron transfer during the redox process. Additionally, the mobility of lattice oxygen in the catalyst ensures the re-oxidation of the reduced surface, thereby enabling the regeneration of the active sites. Xu et al. [98] proposed that CO catalytic oxidation over an α-Mn_2O_3 nano catalyst is dominated by the L-H mechanism at lower temperatures, and turns to the MvK mechanism at higher temperatures, as shown in Figure 18. Morgan et al. [112] found a significant predominance of the MvK mechanism and a relatively minor involvement of the L-H mechanism for CO catalytic oxidation over both undoped and gold-doped $CuMnO_x$ catalysts, and the introduction of gold clearly facilitated the MvK mechanism.

3.3. Interactions between Simultaneous NO_x Catalytic Reduction and CO Catalytic Oxidation on Mn-Based Catalysts

The simultaneous removal of NO_x and CO from industrial fumes involves complex interactions between the NO_x reduction and CO oxidation processes, resulting in some favorable or unfavorable consequences. Nevertheless, these interactions between multiple reactants were determined by various factors, such as the reaction temperature, the concentration of the reactants, and the catalyst properties. Understanding the interactions between various reactants and the influence of reaction conditions on the synergistic removal efficiency was of great significance in designing the catalysts for the simultaneous removal of NO_x and CO.

3.3.1. Effect of CO Oxidation on NO_x Reduction

Gaining insight into how CO oxidation reactants influence NO_x reductions is crucial for improving the efficiency of NO_x removal during the joint removal process. Nevertheless, there is currently no unanimous consensus regarding whether CO catalytic oxidation promotes or inhibits NO_x reduction. Some researchers have proposed that CO catalytic oxidation promotes NO_x reduction. For instance, Zeng et al. [117] confirmed that the CO oxidation reaction has a positive effect on the NO_x reduction reaction. This advantageous

effect could be attributed to the heat that is generated during CO catalytic oxidation, which acts as an ideal heat source to increase the flue gas temperature, thus enhancing the SCR catalytic activity at lower temperatures. Guo et al. [53] demonstrated that the introduction of CO could improve the removal efficiency of NO by facilitating NO adsorption on pre-adsorbed sites. The adsorbed CO serves as a reducing agent, converting NO to N_2, thereby providing an alternative reaction pathway in the SCR process. Nevertheless, some scholars have suggested that CO catalytic oxidation has an inhibitory effect on NO_x reduction. Gui et al. [102] found that the presence of CO has an adverse effect on the NH_3-SCR catalytic activity of $Mn_2Cu_1Al_1O_x$ catalysts. This was mainly due to the competitive adsorption of NH_3 and CO on the active sites. Similarly, Liu et al. [118] observed a noteworthy reduction in NO conversion efficiency in the presence of CO. The decline was ascribed to the simultaneous adsorption of NO and CO on a Mn/Ti catalyst, resulting in a competitive adsorption between CO and NO, as depicted in Figure 19.

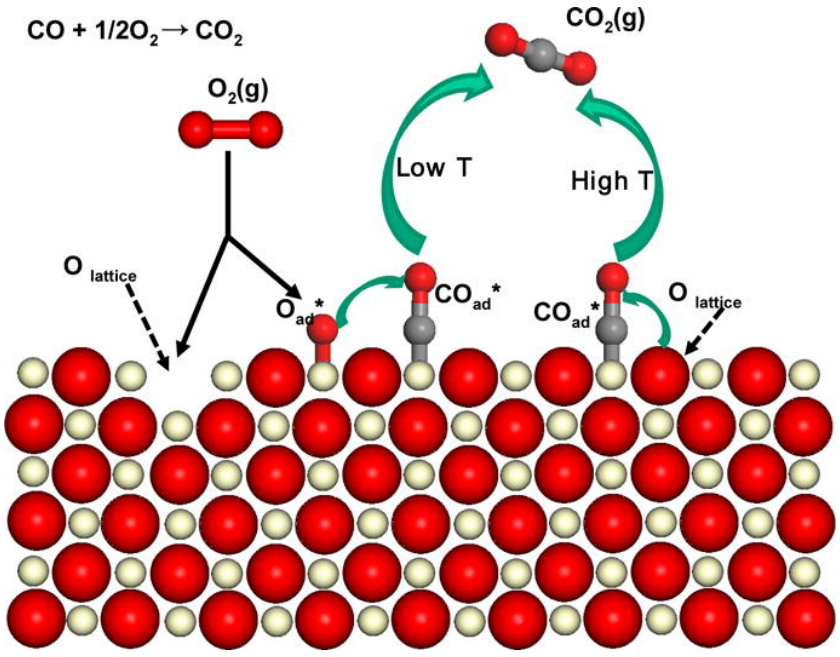

Figure 18. Reaction mechanism for CO catalytic oxidation on an α-Mn_2O_3 catalyst [98].

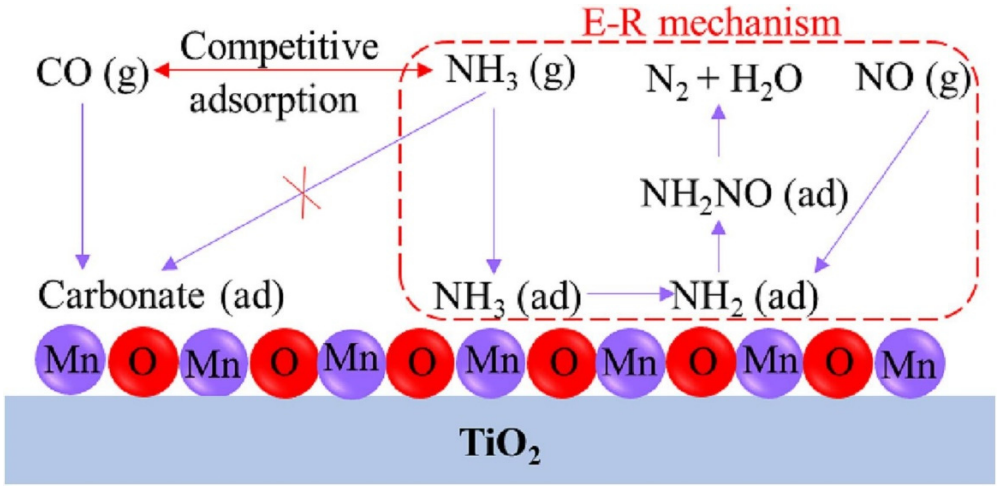

Figure 19. Inhibition mechanism of CO on the NH_3-SCR reaction over a Mn/Ti catalyst [118].

3.3.2. Effect of NH_3-SCR Atmosphere on CO Oxidation

For the simultaneous removal of NO_x and CO in the NH_3-SCR system, the CO conversion rate displays notable distinctions when compared to the individual CO catalytic oxidation reaction, suggesting that NO_x might participate in the CO catalytic oxidation reaction. Zheng et al. [101] found that the CO conversion in a coordinated experiment over a Cu_1Mn_2 catalyst was higher than in a separate experiment, suggesting that NO played a facilitating role in the CO catalytic oxidation reaction. Guo et al. [53] indicated that the adsorption of NO on a CuMn-HZSM-5 catalyst surface generated NO_2^- and $N_2O_2^-$ species, which served as key intermediates for the oxidation of CO to CO_2, as depicted in Figure 20.

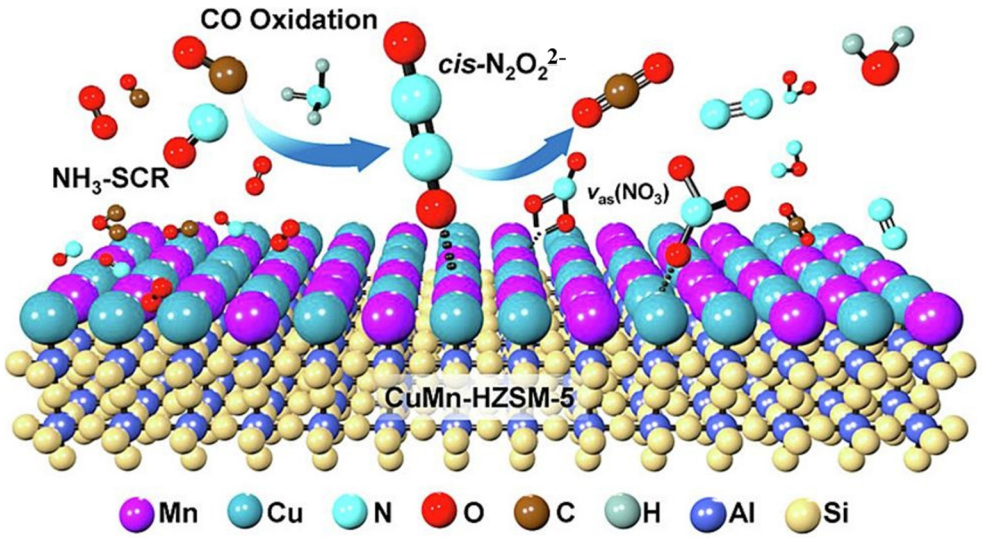

Figure 20. Reaction mechanisms for the selective catalytic reduction of NO and CO oxidation over a CuMn-HZSM-5 catalyst [53].

4. Conclusions and Perspectives

This review provided an in-depth summary of the research progress of Mn-based catalysts in the elimination of NO_x and CO. The catalytic performance, reaction mechanisms, and influence factors of Mn-based catalysts for eliminating NO_x and CO were summarized. Pure MnO_x catalysts exhibit a good catalytic activity for NO_x catalytic reduction and CO oxidation, but with a narrow operating window and poor resistance to toxic substances. The modification of MnO_x catalysts through the incorporation of other metal oxides has been demonstrated to enhance the catalytic activity and widen the operating window. Moreover, the introduction of supports, such as Al_2O_3, TiO_2, and carbon materials, is also an effective strategy for improving the catalytic activity in NH_3-SCR and CO catalytic oxidation reactions. Despite significant advancements in Mn-based catalysts for the removal of NO_x and CO, there remains a pressing need for further in-depth research to develop catalysts with a higher catalytic activity for NO_x reduction and CO oxidation in industrial flue gas conditions. The following aspects could be considered in the future:

(1) Mn-based catalysts exhibit a poor N_2 selectivity in the NH_3-SCR reaction. This is primarily ascribed to the strong oxidizing property of Mn-based catalysts, resulting in the non-selective reduction of NH_3 on the catalyst surface, thereby producing a large amount of the by-products, N_2O. Further research should focus on improving the N_2 selectivity. For enhancing the SCR catalytic properties, it is imperative to inhibit the non-selective catalytic reduction of NH_3, thus enhancing the utilization rate of NH_3.

(2) The resistance to SO_2 and H_2O of Mn-based catalysts is insufficient in both the NH_3-SCR and CO catalytic oxidation reactions. In future studies, scholars should concentrate their efforts on optimizing the active components and developing new structures and morphologies to avoid catalyst deactivation. Furthermore, a crucial

focus should be placed on investigating the regeneration and recycling processes of the catalysts after deactivation.

(3) The interaction mechanism between these two pollutants remains a controversial topic. In further studies, it is essential to employ other methods, such as DFT calculations and reaction kinetics, to gain a better understanding of the reaction processes.

Author Contributions: Conceptualization, X.L. and S.R.; methodology, X.L. and S.R.; data curation, X.L. and L.C.; writing-original draft, X.L.; formal analysis, X.L., Z.C., M.W., H.C. and X.Y.; writing-review & editing, S.R. and H.C.; supervision, S.R.; validation, Z.C. All authors have read and agreed to the published version of the manuscript.

Funding: The current work was financially supported by the National Natural Science Foundation of China (Nos. 52174298 and 52374411) and the Shanxi Provincial Innovation Capacity Support Plan (No. 2023-CX-TD-53).

Institutional Review Board Statement: Not applicable.

Informed Consent Statement: Not applicable.

Data Availability Statement: Not applicable.

Conflicts of Interest: The authors declare no conflict of interest.

References

1. Amoatey, P.; Omidvarborna, H.; Baawain, M.S.; Al-Mamun, A. Emissions and exposure assessments of SO_x, NO_x, PM10/2.5 and trace metals from oil industries: A review study (2000–2018). *Process Saf. Environ. Prot.* **2019**, *123*, 215–228. [CrossRef]
2. Tamilselvan, P.; Nallusamy, N.; Rajkumar, S. A comprehensive review on performance, combustion and emission characteristics of biodiesel fuelled diesel engines. *Renew. Sustain. Energy Rev.* **2017**, *79*, 1134–1159. [CrossRef]
3. Chen, Z.; Ren, S.; Wang, M.; Yang, J.; Chen, L.; Liu, W.; Liu, Q.; Su, B. Insights into samarium doping effects on catalytic activity and SO_2 tolerance of $MnFeO_x$ catalyst for low-temperature NH_3-SCR reaction. *Fuel* **2022**, *321*, 124113. [CrossRef]
4. Fan, Z.; Shi, J.W.; Gao, C.; Gao, G.; Wang, B.; Wang, Y.; He, C.; Niu, C. Gd-modified MnO_x for the selective catalytic reduction of NO by NH_3: The promoting effect of Gd on the catalytic performance and sulfur resistance. *Chem. Eng. J.* **2018**, *348*, 820–830. [CrossRef]
5. Li, Y.; Jiang, L.; Zhao, G.; Guo, L.; Tian, C.; Tao, X.; Du, M.; Nan, B.; Liu, X.; Li, L. Enhancing the low-temperature CO oxidation over Pt/Y_2O_3 catalyst: The effects of Pt dispersion and support basicity on the catalytic performance. *Appl. Surf. Sci.* **2023**, *614*, 156210. [CrossRef]
6. Li, X.; Ren, S.; Chen, Z.; Chen, L.; Wang, M.; Wang, L.; Wang, A. Promoting mechanism of CuO on catalytic performance of CeFe catalyst for simultaneous removal of NO_x and CO. *Fuel* **2023**, *347*, 128435. [CrossRef]
7. Hu, Y.; Griffiths, K.; Norton, P.R. Surface science studies of selective catalytic reduction of NO: Progress in the last ten years. *Surf. Sci.* **2009**, *603*, 1740–1750. [CrossRef]
8. Du, Y.; Gao, F.; Zhou, Y.; Yi, H.; Tang, X.; Qi, Z. Recent advance of $CuO\text{-}CeO_2$ catalysts for catalytic elimination of CO and NO. *J. Environ. Chem. Eng.* **2021**, *9*, 106372. [CrossRef]
9. Yahiro, H.; Iwamoto, M. Copper ion-exchanged zeotile catalysts in deNO_x reaction. *Appl. Catal. A-Gen.* **2001**, *222*, 163–181. [CrossRef]
10. Xue, J.; Wang, X.; Qi, G.; Wang, J.; Shen, M.; Li, W. Characterization of copper species over Cu/SAPO-34 in selective catalytic reduction of NO_x with ammonia: Relationships between active Cu sites and de-NO_x performance at low temperature. *J. Catal.* **2013**, *297*, 56–64. [CrossRef]
11. Ma, J.; Chang, S.; Yu, F.; Lai, H.; Zhao, Y. Research progress on sulfur deactivation and regeneration over Cu-CHA zeolite catalyst. *Catalysts* **2022**, *12*, 1499. [CrossRef]
12. Liu, X.; Zhang, X.; Meng, C. Coadsorption interfered CO oxidation over atomically dispersed Au on *h*-BN. *Molecules* **2022**, *27*, 3627. [CrossRef] [PubMed]
13. Lou, Y.; Liu, J. CO oxidation on metal oxide supported single Pt atoms: The role of the support. *Ind. Eng. Chem. Res.* **2017**, *56*, 6916–6925. [CrossRef]
14. Krishnan, R.; Wu, S.Y.; Chen, H.T. Single Pt atom supported on penta-graphene as an efficient catalyst for CO oxidation. *Phys. Chem. Chem. Phys.* **2019**, *21*, 12201–12208. [CrossRef] [PubMed]
15. Liu, X.; Xu, M.; Wan, L.; Zhu, H.; Yao, K.; Linguerri, R.; Chambaud, G.; Han, Y.; Meng, C. Superior catalytic performance of atomically dispersed palladium on graphene in CO oxidation. *ACS Catal.* **2020**, *10*, 3084–3093. [CrossRef]
16. Prasad, R.; Singh, P. A review on CO oxidation over copper chromite catalyst. *Catal. Rev.* **2012**, *54*, 224–279. [CrossRef]
17. Raphulu, M.; Mcpherson, J.; Pattrick, G.; Ntho, T.; Mokoena, L.; Moma, J. Co oxidation: Deactivation of Au/TiO_2 catalysts during storage. *Gold Bull.* **2009**, *42*, 328–336. [CrossRef]

18. Xanthopoulou, G.; Vekinis, G. Investigation of catalytic oxidation of carbon monoxide over a Cu-Cr-oxide catalyst made by self-propagating high-temperature synthesis. *Appl. Catal. B-Environ.* **1998**, *19*, 37–44. [CrossRef]
19. Schlatter, J.; Klimisch, R.; Taylor, K. Exhaust catalysts: Appropriate conditions for comparing platinum and base metal. *Science* **1973**, *179*, 798–800. [CrossRef]
20. Damma, D.; Boningari, T.; Ettireddy, P.R.; Reddy, B.M.; Smirniotis, P.G. Direct decomposition of NO_x over TiO_2 supported transition metal oxides at low temperatures. *Ind. Eng. Chem. Res.* **2018**, *57*, 16615–16621. [CrossRef]
21. Chen, L.; Ren, S.; Liu, W.; Yang, J.; Chen, Z.; Wang, M.; Liu, Q. Low-temperature NH_3-SCR activity of M (M = Zr, Ni and Co) doped MnO_x supported biochar catalysts. *J. Environ. Chem. Eng.* **2021**, *9*, 106504. [CrossRef]
22. Thirupathi, B.; Smirniotis, P.G. Co-doping a metal (Cr, Fe, Co, Ni, Cu, Zn, Ce, and Zr) on Mn/TiO_2 catalyst and its effect on the selective reduction of NO with NH_3 at low-temperatures. *Appl. Catal. B-Environ.* **2011**, *110*, 195–206. [CrossRef]
23. Fan, L.; Shi, J.; Niu, C.; Wang, B.; He, C.; Cheng, Y. The insight into the role of Al_2O_3 in promoting the SO_2 tolerance of MnO_x for low-temperature selective catalytic reduction of NO_x with NH_3. *Chem. Eng. J.* **2020**, *398*, 125572. [CrossRef]
24. Li, G.; Mao, D.; Chao, M.; Li, G.; Yu, J.; Guo, X. Low-temperature NH_3-SCR of NO_x over $MnCeO_x/TiO_2$ catalyst: Enhanced activity and SO_2 tolerance by modifying TiO_2 with Al_2O_3. *J. Rare Earth.* **2021**, *39*, 805–816. [CrossRef]
25. Meng, D.; Zhan, W.; Guo, Y.; Wang, L.; Lu, G. A highly effective catalyst of Sm-MnO_x for the NH_3-SCR of NO_x at low temperature: Promoting role of Sm and its catalytic performance. *ACS Catal.* **2015**, *5*, 5973–5983. [CrossRef]
26. Huang, L.; Hu, X.; Yuan, S.; Li, H.; Yan, T.; Shi, L.; Zhang, D. Photocatalytic preparation of nanostructured MnO_2-$(Co_3O_4)/TiO_2$ hybrids: The formation mechanism and catalytic application in SCR deNO_x reaction. *Appl. Catal. B-Environ.* **2017**, *203*, 778–788. [CrossRef]
27. Yang, S.; Qi, F.; Xiong, S.; Dang, H.; Liao, Y.; Wong, P.K.; Li, J. MnO_x supported on Fe-Ti spinel: A novel Mn based low temperature SCR catalyst with a high N_2 selectivity. *Appl. Catal. B-Environ.* **2016**, *181*, 570–580. [CrossRef]
28. He, G.; Gao, M.; Peng, Y.; Yu, Y.; Shan, W.; He, H. Superior oxidative dehydrogenation performance toward NH_3 determines the excellent low-temperature NH_3-SCR activity of Mn-based catalysts. *Environ. Sci. Technol.* **2021**, *55*, 6995–7003. [CrossRef]
29. Tang, X.; Hao, J.; Xu, W.; Li, J. Low temperature selective catalytic reduction of NO_x with NH_3 over amorphous MnO_x catalysts prepared by three methods. *Catal. Commun.* **2007**, *8*, 329–334. [CrossRef]
30. Kang, M.; Park, E.D.; Kim, J.M.; Yie, J.E. Manganese oxide catalysts for NO_x reduction with NH_3 at low temperatures. *Appl. Catal. A-Gen.* **2007**, *327*, 261–269. [CrossRef]
31. Tang, X.; Li, J.; Sun, L.; Hao, J. Origination of N_2O from NO reduction by NH_3 over β-MnO_2 and α-Mn_2O_3. *Appl. Catal. B-Environ.* **2010**, *99*, 156–162. [CrossRef]
32. Hayashi, E.; Yamaguchi, Y.; Kamata, K.; Tsunoda, N.; Kumagai, Y.; Oba, F.; Hara, M. Effect of MnO_2 crystal structure on aerobic oxidation of 5-hydroxymethylfurfural to 2,5-furandicarboxylic acid. *J. Am. Chem. Soc.* **2019**, *141*, 890–900. [CrossRef] [PubMed]
33. Robinson, D.M.; Go, Y.B.; Mui, M.; Gardner, G.; Zhang, Z.; Mastrogiovanni, D.; Garfunkel, E.; Li, J.; Greenblatt, M.; Dismukes, G.C. Photochemical water oxidation by crystalline polymorphs of manganese oxides: Structural requirements for catalysis. *J. Am. Chem. Soc.* **2013**, *135*, 3494–3501. [CrossRef]
34. Yang, R.; Fan, Y.; Ye, R.; Tang, Y.; Cao, X.; Yin, Z.; Zeng, Z. MnO_2-based materials for environmental applications. *Adv. Mater.* **2021**, *33*, 2004862. [CrossRef]
35. Li, Y.F.; Zhu, S.C.; Liu, Z.P. Reaction network of layer-to-tunnel transition of MnO_2. *J. Am. Chem. Soc.* **2016**, *138*, 5371–5379. [CrossRef] [PubMed]
36. Sun, C.; Zhang, Y.; Song, S.; Xue, D. Tunnel-dependent supercapacitance of MnO_2: Effects of crystal structure. *J. Appl. Crystallogr.* **2013**, *46*, 1128–1135. [CrossRef]
37. Gong, P.; Xie, J.; Fang, D.; Han, D.; He, F.; Li, F.; Qi, K. Effects of surface physicochemical properties on NH_3-SCR activity of MnO_2 catalysts with different crystal structures. *Chin. J. Catal.* **2017**, *38*, 1925–1934. [CrossRef]
38. Dai, Y.; Li, J.H.; Peng, Y.; Tang, X.F. Effects of MnO_2 crystal structure and surface property on the NH_3-SCR reaction at low temperature. *Acta Phys.-Chim Sin.* **2012**, *28*, 1771–1776.
39. Yang, J.; Ren, S.; Su, B.; Zhou, Y.; Hu, G.; Jiang, L.; Cao, J.; Liu, W.; Yao, L.; Kong, M. Insight into N_2O formation over different crystal phases of MnO_2 during low-temperature NH_3-SCR of NO. *Catal. Lett.* **2021**, *151*, 2964–2971. [CrossRef]
40. Zhang, M.; Wang, J.; Zhang, Y.; Zhang, M.; Zhou, Y.; Phoutthavong, T.; Liang, P.; Zhang, H. Simultaneous removal of NO and Hg^0 in flue gas over Co-Ce oxide modified rod-like MnO_2 catalyst: Promoting effect of Co doping on activity and SO_2 resistance. *Fuel* **2020**, *276*, 118018. [CrossRef]
41. Luo, S.; Zhou, W.; Xie, A.; Wu, F.; Yao, C.; Li, X.; Zuo, S.; Liu, T. Effect of MnO_2 polymorphs structure on the selective catalytic reduction of NO_x with NH_3 over TiO_2-Palygorskite. *Chem. Eng. J.* **2016**, *286*, 291–299. [CrossRef]
42. Wang, J.; Zhu, J.; Zhou, X.; Du, Y.; Huang, W.; Liu, J.; Zhang, W.; Shi, J.; Chen, H. Nanoflower-like weak crystallization manganese oxide for efficient removal of low-concentration NO at room temperature. *J. Mater. Chem. A* **2015**, *3*, 7631–7638. [CrossRef]
43. Liu, J.; Wei, Y.; Li, P.Z.; Zhang, P.; Su, W.; Sun, Y.; Zou, R.; Zhao, Y. Experimental and theoretical investigation of mesoporous MnO_2 nanosheets with oxygen vacancies for high-efficiency catalytic deNO_x. *ACS Catal.* **2018**, *8*, 3865–3874. [CrossRef]
44. Li, Y.; Li, Y.; Wan, Y.; Zhan, S.; Guan, Q.; Tian, Y. Structure-performance relationships of MnO_2 nanocatalyst for the low-temperature SCR removal of NO_x under ammonia. *RSC Adv.* **2016**, *6*, 54926–54937. [CrossRef]
45. Gao, J.; Han, Y.; Mu, J.; Wu, S.; Tan, F.; Shi, Y.; Li, X. 2D, 3D mesostructured silicas templated mesoporous manganese dioxide for selective catalytic reduction of NO_x with NH_3. *J. Colloid Interface Sci.* **2018**, *516*, 254–262. [CrossRef] [PubMed]

46. Chen, S.; Yan, Q.; Zhang, C.; Wang, Q. A novel highly active and sulfur resistant catalyst from Mn-Fe-Al layered double hydroxide for low temperature NH_3-SCR. *Catal. Today* **2019**, *327*, 81–89. [CrossRef]
47. Kapteijn, F.; Singoredjo, L.; Andreini, A.; Moulijn, J.A. Activity and selectivity of pure manganese oxides in the selective catalytic reduction of nitric oxide with ammonia. *Appl. Catal. B-Environ.* **1994**, *3*, 173–189. [CrossRef]
48. Yang, J.; Ren, S.; Zhou, Y.; Su, Z.; Liu, Q. In situ IR comparative study on N_2O formation pathways over different valence states manganese oxides catalysts during NH_3-SCR of NO. *Chem. Eng. J.* **2020**, *397*, 125446. [CrossRef]
49. Wan, Y.; Zhao, W.; Tang, Y.; Li, L.; Wang, H.; Cui, Y.; Gu, J.; Li, Y.; Shi, J. Ni-Mn bi-metal oxide catalysts for the low temperature SCR removal of NO with NH_3. *Appl. Catal. B-Environ.* **2014**, *148*, 114–122. [CrossRef]
50. Zhang, D.; Zhang, L.; Shi, L.; Fang, C.; Li, H.; Gao, R.; Huang, L.; Zhang, J. In situ supported MnO_x-CeO_x on carbon nanotubes for the low-temperature selective catalytic reduction of NO with NH_3. *Nanoscale* **2013**, *5*, 1127–1136. [CrossRef]
51. Pappas, D.K.; Boningari, T.; Boolchand, P.; Smirniotis, P.G. Novel manganese oxide confined interweaved titania nanotubes for the low-temperature selective catalytic reduction (SCR) of NO_x by NH_3. *J. Catal.* **2016**, *334*, 1–13. [CrossRef]
52. Chen, Z.; Ren, S.; Xing, X.; Li, X.; Chen, L.; Wang, M. Unveiling the inductive strategy of different precipitants on $MnFeO_x$ catalyst for low-temperature NH_3-SCR reaction. *Fuel* **2023**, *335*, 126986. [CrossRef]
53. Guo, Y.; Zheng, Y.; Peng, Y.; Yue, T.; Zhu, T. Bifunctional catalyst of CuMn-HZSM-5 for selective catalytic reduction of NO and CO oxidation under oxygen atmosphere. *Chem. Eng. J.* **2023**, *462*, 142113. [CrossRef]
54. Wang, C.; Gao, F.; Ko, S.; Liu, H.; Yi, H.; Tang, X. Structural control for inhibiting SO_2 adsorption in porous MnCe nanowire aerogel catalysts for low-temperature NH_3-SCR. *Chem. Eng. J.* **2022**, *434*, 134729. [CrossRef]
55. Han, L.; Gao, M.; Feng, C.; Shi, L.; Zhang, D. Fe_2O_3-CeO_2@Al_2O_3 Nanoarrays on Al-mesh as SO_2-tolerant monolith catalysts for NO_x reduction by NH_3. *Environ. Sci. Technol.* **2019**, *53*, 5946–5956. [CrossRef] [PubMed]
56. Yang, J.; Ren, S.; Zhang, T.S.; Su, Z.H.; Long, H.M.; Kong, M.; Yao, L. Iron doped effects on active sites formation over activated carbon supported Mn-Ce oxide catalysts for low-temperature SCR of NO. *Chem. Eng. J.* **2020**, *379*, 122398. [CrossRef]
57. Lia, H.K.; Liaw, B.J.; Chen, Y.Z. Removal of CO in excess hydrogen over $CuO/Ce_{1-x}Mn_xO_2$ catalysts. *Chem. Eng. J.* **2011**, *172*, 452–458.
58. Shi, Y.; Yi, H.; Gao, F.; Zhao, S.; Xie, Z.; Tang, X. Evolution mechanism of transition metal in NH_3-SCR reaction over Mn-based bimetallic oxide catalysts: Structure-activity relationships. *J. Hazard. Mater.* **2021**, *413*, 125361. [CrossRef]
59. Kang, H.; Wang, J.; Zheng, J.; Chu, W.; Tang, C.; Ji, J.; Ren, R.; Wu, M.; Jing, F. Solvent-free elaboration of Ni-doped MnO_x catalysts with high performance for NH_3-SCR in low and medium temperature zones. *Mol. Catal.* **2021**, *501*, 111376. [CrossRef]
60. Jiang, B.; Deng, B.; Zhang, Z.; Wu, Z.; Tang, X.; Yao, S.; Lu, H. Effect of Zr addition on the low-temperature SCR activity and SO_2 tolerance of Fe-Mn/Ti catalysts. *J. Phys. Chem. C* **2014**, *118*, 14866–14875. [CrossRef]
61. Long, L.; Tian, S.; Zhao, Y.; Zhang, X.; Luo, W.; Yao, X. Promotional effects of Nb^{5+} and Fe^{3+} co-doping on catalytic performance and SO_2 resistance of MnO_x-CeO_2 low-temperature denitration catalyst. *J. Colloid Interface Sci.* **2023**, *648*, 876–888. [CrossRef] [PubMed]
62. Zeng, Y.; Lyu, F.; Wang, Y.; Zhang, S.; Zhong, Q.; Zhong, Z. New insight on N_2O formation over MnO_x/TiO_2 catalysts for selective catalytic reduction of NO_x with NH_3. *Mol. Catal.* **2022**, *525*, 112356. [CrossRef]
63. Liu, X.; Yu, Q.; Chen, H.; Jiang, P.; Shen, Z. The promoting effect of S-doping on the NH_3-SCR performance of MnO/TiO_2 catalyst. *Appl. Surf. Sci.* **2019**, *508*, 144694. [CrossRef]
64. Yang, G.; Zhao, H.; Luo, X.; Shi, K.; Zhao, H.; Wang, W.; Chen, Q.; Fan, H.; Wu, T. Promotion effect and mechanism of the addition of Mo on the enhanced low temperature SCR of NO_x by NH_3 over MnO_x/γ-Al_2O_3 catalysts. *Appl. Catal. B-Environ.* **2019**, *245*, 743–752. [CrossRef]
65. Kijlstra, W.S.; Brands, D.S.; Poels, E.K.; Bliek, A. Kinetics of the selective catalytic reduction of NO with NH_3 over MnO_x/Al_2O_3 catalysts at low temperature. *Catal. Today* **1999**, *50*, 133–140. [CrossRef]
66. Kijlstra, W.S.; Brands, D.S.; Smit, H.I.; Poels, E.K.; Bliek, A. Mechanism of the selective catalytic reduction of NO with NH_3 over MnO_x/Al_2O_3. *J.Catal.* **1997**, *171*, 219–230. [CrossRef]
67. Kong, T.; Chen, L.; Ding, S.; Yang, F.; Dong, L. Enhanced low-temperature NH_3-SCR performance of MnO_x/CeO_2 catalysts by optimal solvent effect. *Appl. Surf. Sci.* **2017**, *420*, 407–415.
68. Hsu, L.; Tsai, M.; Lu, Y.; Chen, H. Computional inverstigation of CO adsorption and oxidation on Mn/CeO_2(111) surfface. *J. Phys. Chem. C.* **2013**, *117*, 433–441. [CrossRef]
69. Li, J.; Zhu, P.; Zhou, R. Effect of the preparation method on the performance of CuO-MnO_x-CeO_2 catalysts for selective oxidation of CO in H_2-rich streams. *J. Power Sources* **2011**, *196*, 9590–9598. [CrossRef]
70. Vasilyeva, M.; Rudnev, V.; Ustinov, A.; Tsvetnov, M. Formation, composition, structure, and catalytic activity in CO oxidation of SiO_2 + TiO_2/Ti composite before and after modification by MnO_x or CoO_x. *Surf. Coat. Technol.* **2015**, *275*, 84–89. [CrossRef]
71. Shen, B.; Zhang, X.; Ma, H.; Yao, Y.; Liu, T. A comparative study of Mn/CeO_2, Mn/ZrO_2 and Mn/Ce-ZrO_2 for low temperature selective catalytic reduction of NO with NH_3 in the presence of SO_2 and H_2O. *J. Environ. Sci.* **2013**, *25*, 791–800. [CrossRef] [PubMed]
72. Jia, B.; Guo, J.; Luo, H.; Shu, S.; Fang, N.; Li, J. Study of NO removal and resistance to SO_2 and H_2O of MnO_x/TiO_2, MnO_x/ZrO_2 and MnO_x/ZrO_2-TiO_2. *Appl. Catal. A-Gen.* **2018**, *553*, 82–90. [CrossRef]

73. Yao, L.; Liu, Q.; Mossin, S.; Nielsen, D.; Kong, M.; Jiang, L.; Yang, J.; Ren, S.; Wen, J. Promotional effects of nitrogen doping on catalytic performance over manganese-containing semi-coke catalysts for the NH_3-SCR at low temperatures. *J. Hazard. Mater.* **2020**, *387*, 121704. [CrossRef] [PubMed]
74. Li, J.; Zhang, C.; Li, Q.; Gao, T.; Yu, S.; Tan, P.; Fang, Q.; Chen, G. Promoting mechanism of SO_2 resistance performance by anatase TiO_2 {001} facets on Mn-Ce/TiO_2 catalysts during NH_3-SCR reaction. *Chem. Eng. Sci.* **2022**, *251*, 117438. [CrossRef]
75. Ettireddy, P.R.; Ettireddy, N.; Mamedov, S.; Boolchand, P.; Smirniotis, P.G. Surface characterization studies of TiO_2 supported manganese oxide catalysts for low temperature SCR of NO with NH_3. *Appl. Catal. B-Environ.* **2007**, *76*, 123–134. [CrossRef]
76. Kim, Y.J.; Kwon, H.J.; Nam, I.S.; Choung, J.W.; Kil, J.K.; Kim, H.J.; Cha, M.S.; Yeo, G.K. High deNO_x performance of Mn/TiO_2 catalyst by NH_3. *Catal. Today* **2010**, *151*, 244–250. [CrossRef]
77. Smirniotis, P.G.; Peña, D.A.; Uphade, B.S. Low-temperature selective catalytic reduction (SCR) of NO with NH_3 by using Mn, Cr, and Cu oxides supported on Hombikat TiO_2. *Angew. Chem. Int. Ed.* **2001**, *40*, 2479–2482. [CrossRef]
78. Yao, X.; Kong, T.; Yu, S.; Li, L.; Yang, F.; Dong, L. Influence of different supports on the physicochemical properties and denitration performance of the supported Mn-based catalysts for NH_3-SCR at low temperature. *Appl. Surf. Sci.* **2017**, *402*, 208–217. [CrossRef]
79. Jin, R.; Liu, Y.; Wu, Z.; Wang, H.; Gu, T. Low-temperature selective catalytic reduction of NO with NH_3 over MnCe oxides supported on TiO_2 and Al_2O_3: A comparative study. *Chemosphere* **2010**, *78*, 1160–1166. [CrossRef]
80. Li, L.; Ji, J.; Tan, W.; Song, W.; Wang, X.; Wei, X.; Guo, K.; Zhang, W.; Tang, C.; Dong, L. Enhancing low-temperature NH_3-SCR performance of Fe-Mn/CeO_2 catalyst by Al_2O_3 modification. *J. Rare Earth.* **2022**, *40*, 1454–1461. [CrossRef]
81. Gao, L.; Li, C.; Li, S.; Zhang, W.; Du, X.; Huang, L.; Zhu, Y.; Zhai, Y.; Zeng, G. Superior performance and resistance to SO_2 and H_2O over CoO_x-modified MnO_x/biomass activated carbons for simultaneous Hg^0 and NO removal. *Chem. Eng. J.* **2019**, *371*, 781–795. [CrossRef]
82. Su, Z.; Ren, S.; Zhang, T.; Yang, J.; Zhou, Y.; Yao, L. Effects of PbO poisoning on Ce-Mn/AC catalyst for low-temperature selective catalytic reduction of NO with NH_3. *J. Iron Steel Res. Int.* **2021**, *28*, 133–139. [CrossRef]
83. Su, Y.; Fan, B.; Wang, L.; Liu, Y.; Huang, B.; Fu, M.; Chen, L.; Ye, D. MnO_x supported on carbon nanotubes by different methods for the SCR of NO with NH_3. *Catal. Today* **2013**, *201*, 115–121. [CrossRef]
84. Xiao, X.; Sheng, Z.; Yang, L.; Dong, F. Low-temperature selective catalytic reduction of NO_x with NH_3 over a manganese and cerium oxide/graphene composite prepared by a hydrothermal method. *Catal. Sci. Technol.* **2016**, *6*, 1507–1514. [CrossRef]
85. Jiang, L.; Xu, Y.; Jiang, W.; Pu, Y.; Yang, L.; Dai, Z.; Yao, L. The promotion of NH_3-SCR performance by AC addition on Mn-Fe/Z catalyst. *Sep. Purif. Technol.* **2023**, *322*, 124274. [CrossRef]
86. Liang, S.; Teng, F.; Bulgan, G.; Zong, R.; Zhu, Y. Effect of phase structure of MnO_2 nanorod catalyst on the activity for CO oxidation. *J. Phys. Chem. C* **2008**, *112*, 5307–5315. [CrossRef]
87. Xu, R.; Wang, X.; Wang, D.; Zhou, K.; Li, Y. Surface structure effects in nanocrystal MnO_2 and Ag/MnO_2 catalytic oxidation of CO. *J. Catal.* **2006**, *237*, 426–430. [CrossRef]
88. Frey, K.; Iablokov, V.; Sáfrán, G.; Osán, J.; Sajó, I.; Szukiewicz, R.; Chenakin, S.; Kruse, N. Nanostructured MnO_x as highly active catalyst for CO oxidation. *J. Catal.* **2012**, *287*, 30–36. [CrossRef]
89. Wang, X.; Huo, W.; Xu, Y.; Guo, Y.; Jia, Y. Modified hierarchical birnessite-type manganese oxide nanomaterials for CO catalytic oxidation. *New J. Chem.* **2018**, *42*, 13803–13812. [CrossRef]
90. Ramesh, K.; Chen, L.; Chen, F.; Liu, Y.; Wang, Z.; Han, Y.F. Re-investigating the CO oxidation mechanism over unsupported MnO, Mn_2O_3 and MnO_2 catalysts. *Catal. Today* **2008**, *131*, 477–482. [CrossRef]
91. Cai, L.N.; Guo, Y.; Lu, A.H.; Branton, P.; Li, W.C. The choice of precipitant and precursor in the co-precipitation synthesis of copper manganese oxide for maximizing carbon monoxide oxidation. *J. Mol. Catal. A-Chem.* **2012**, *360*, 35–41. [CrossRef]
92. Pan, H.; Chen, X.; López-Cartes, C.; Martínez-López, J.; Bu, E.; Delgado, J.J. Hydrothermal synthesis and characterization of Cu-MnO_x catalysts for CO oxidation: Effect of Cu: Mn molar ratio on their structure and catalytic activity. *Catal. Today* **2023**, *418*, 114085. [CrossRef]
93. Zhang, X.; Deng, Y.; Tian, P.; Shang, H.; Xu, J.; Han, Y. Dynamic active sites over binary oxide catalysts: *In situ*/operando spectroscopic study of low-temperature CO oxidation over MnO_x-CeO_2 catalysts. *Appl. Catal. B-Environ.* **2016**, *191*, 179–191. [CrossRef]
94. Dong, S.; Wang, J.; Tang, X.; Li, J.; Zhang, X.; Liu, B. Low-temperature and stable CO oxidation of *in-situ* grown monolithic Mn_3O_4/TiO_2 catalysts. *J. Alloys Compd.* **2021**, *855*, 157444. [CrossRef]
95. Camposeco, R.; Castillo, S.; Nava, N.; Medina, J.C.; Zanella, R. Effect of gold nanoparticles on MnO_x/TiO_2 nanostructures for improving the CO oxidation at low temperature. *Top. Catal.* **2020**, *63*, 492–503. [CrossRef]
96. Dey, S.; Dhal, G.C.; Mohan, D.; Prasad, R. Characterization and activity of $CuMnO_x$/γ-Al_2O_3 catalyst for oxidation of carbon monoxide. *Mater. Discov.* **2017**, *8*, 26–34. [CrossRef]
97. Li, L.; Han, W.; Dong, F.; Zong, L.; Tang, Z.; Zhang, J. Controlled pore size of ordered mesoporous Al_2O_3-supported Mn/Cu catalysts for CO oxidation. *Microporous Mesoporous Mater.* **2017**, *249*, 1–9. [CrossRef]
98. Xu, J.; Deng, Y.Q.; Luo, Y.; Mao, W.; Yang, X.J.; Han, Y.F. Operando Raman spectroscopy and kinetic study of low-temperature CO oxidation on an α-Mn_2O_3 nanocatalyst. *J. Catal.* **2013**, *300*, 225–234. [CrossRef]
99. Xu, G.; Guo, X.; Cheng, X.; Yu, J.; Fang, B. A review of Mn-based catalysts for low-temperature NH_3-SCR: NO_x removal and H_2O/SO_2 resistance. *Nanoscale* **2021**, *23*, 7052–7080. [CrossRef]

100. Li, X.; Ren, S.; Chen, Z.; Jiang, Y.; Wang, M.; Wang, L.; Liu, M. Unraveling the morphology and crystal plane dependence of bifunctional MnO_2 catalyst for simultaneous removal of NO and CO at low temperature. *Sep. Purif. Technol.* **2023**, *325*, 124760. [CrossRef]
101. Zheng, Y.; Guo, Y.; Xu, X.; Zhu, T. Study of Cu/Mn catalysts for coreactions of NH_3-SCR and CO oxidation. *Catal. Lett.* **2022**, *152*, 1752–1759. [CrossRef]
102. Gui, R.; Xiao, J.; Gao, Y.; Li, Y.; Zhu, T.; Wang, Q. Simultaneously achieving selective catalytic reduction of NO_x with NH_3 and catalytic oxidation of CO with O_2 over one finely optimized bifunctional catalyst $Mn_2Cu_1Al_1O_x$ at low temperatures. *Appl. Catal. B-Environ.* **2022**, *306*, 121104. [CrossRef]
103. Wang, J.; Xing, Y.; Su, W.; Li, K.; Zhang, W. Bifunctional Mn-Cu-CeO_x/γ-Al_2O_3 catalysts for low-temperature simultaneous removal of NO_x and CO. *Fuel* **2022**, *321*, 124050. [CrossRef]
104. Guo, J.; Xiao, J.; Gui, R.; Gao, Y.; Wang, Q. Efficient simultaneous removal of NO_x and CO at low temperatures over integrated $Mn_2Co_1O_x$/iron mesh monolithic catalyst via NH_3-SCR coupling with CO oxidation reactions. *Chem. Eng. J.* **2023**, *465*, 142611. [CrossRef]
105. Han, L.; Cai, S.; Gao, M.; Hasegawa, J.; Wang, P.; Zhang, J.; Shi, L.; Zhang, D. Selective catalytic reduction of NO_x with NH_3 by using novel catalysts: State of the art and future prospects. *Chem. Rev.* **2019**, *119*, 10916–10976. [CrossRef] [PubMed]
106. Marbán, G.; Valdés-Solís, T.; Fuertes, A.B. Mechanism of low-temperature selective catalytic reduction of NO with NH_3 over carbon-supported Mn_3O_4: Role of surface NH_3 species: SCR mechanism. *J. Catal.* **2004**, *226*, 138–155. [CrossRef]
107. Xu, S.; Chen, J.; Li, Z.; Liu, Z. Highly ordered mesoporous MnO_x catalyst for the NH_3-SCR of NO_x at low temperatures. *Appl. Catal. A-Gen.* **2023**, *649*, 118966. [CrossRef]
108. Liu, C.; Shi, J.W.; Gao, C.; Niu, C. Manganese oxide-based catalysts for low-temperature selective catalytic reduction of NO_x with NH_3: A review. *Appl.Catal. A-Gen.* **2016**, *522*, 54–69. [CrossRef]
109. Wei, L.; Cui, S.; Guo, H.; Ma, X. Study on the role of Mn species in low temperature SCR on MnO_x/TiO_2 through experiment and DFT calculation. *Mol. Catal.* **2018**, *445*, 102–110. [CrossRef]
110. Freund, H.J.; Meijer, G.; Scheffler, M.; Schlögl, R.; Wolf, M. CO oxidation as a prototypical reaction for heterogeneous processes. *Angew. Chem. Int. Ed.* **2011**, *50*, 10064–10094. [CrossRef]
111. Stampfl, C.; Scheffler, M. Density-functional theory study of the catalytic oxidation of CO over transition metal surfaces. *Surf. Sci.* **1999**, *433*, 119–126. [CrossRef]
112. Morgan, K.; Cole, K.J.; Goguet, A.; Hardacre, C.; Hutchings, G.J.; Maguire, N.; Shekhtman, S.O.; Taylor, S.H. TAP studies of CO oxidation over $CuMnO_x$ and Au/$CuMnO_x$ catalysts. *J.Catal.* **2010**, *276*, 38–48. [CrossRef]
113. Cacciatore, M.; Rutigliano, M.; Billing, G. Eley-Rideal and Langmuir-Hinshelwood recombination coefficients for oxygen on silica surfaces. *J. Thermophys. Heat Transf.* **1999**, *13*, 195–203. [CrossRef]
114. Dey, S.; Dhal, G.C.; Mohan, D.; Prasad, R. Effect of preparation conditions on the catalytic activity of $CuMnO_x$ catalysts for CO oxidation. *Bull. Chem. React. Eng. Catal.* **2017**, *12*, 437–451. [CrossRef]
115. Prasad, R.; Singh, P. A novel route of single step reactive calcination of copper salts far below their decomposition temperatures for synthesis of highly active catalysts. *Catal. Sci. Technol.* **2013**, *3*, 3326–3334. [CrossRef]
116. Dey, S.; Dhal, G.C.; Mohan, D.; Prasad, R. Effect of various metal oxides phases present in $CuMnO_x$ catalyst for selective CO oxidation. *Mater. Discov.* **2018**, *12*, 63–71. [CrossRef]
117. Zeng, Y.; Rong, W.; Zhang, S.; Wang, Y.; Zhong, Q. Promoting NH_3-SCR denitration via CO oxidation over CuO promoted V_2O_5-WO_3/TiO_2 catalysts under oxygen-rich conditions. *Fuel* **2022**, *323*, 124357. [CrossRef]
118. Liu, L.; Liu, T.; Zhou, Y.; Zheng, X.; Su, S.; Yu, J.; Xiang, J. Inhibitory effect of CO on NH_3-SCR of NO over Mn/TiO_2 catalyst at low temperature: Inhibitory mechanism investigated by in situ DRIFTS. *Appl. Surf. Sci.* **2023**, *638*, 158003. [CrossRef]